DEVELOPMENT AND IMPLEMENTATION OF IMPROVED EXTERNAL BALANCE LOAD MEASUREMENTS

A Thesis

by

NATHANIEL JACOB FRANKLIN

Submitted to the Office of Graduate and Professional Studies of
Texas A&M University
in partial fulfillment of the requirements for the degree of

MASTER OF SCIENCE

Chair of Committee,	Edward White
Committee Members,	Douglas Allaire
	Sharath Girimaji
Head of Department,	Rodney Bowersox

August 2019

Major Subject: Aerospace Engineering

ABSTRACT

The Texas A&M Oran W. Nicks Low Speed Wind Tunnel (LSWT) uses a large pyramidal-type external force balance to measure aerodynamic loads. This balance was designed and constructed in the 1940s and measures the six wind frame aerodynamic forces and moments through a system of levers and pushrods that terminate in six movable poise weights and individual analog controllers. These systems were updated in the mid 1970s to use vacuum tubes, double wound motors, rotary encoders, and analog linear potentiometers. Although antiquated, these analog components provide outstanding sensitivity and linearity. However, the fragility, tight tuning margins, and overall age of the system has proven troublesome for the LSWT. The objective of this thesis is to design, implement, and provide a preliminary calibration of new measurement electronics that improve sensor reaction time, robustness, and ease of use while taking advantage of existing mechanical structure. This updated system must meet certain minimum requirements, namely, it must be at least as accurate as the original system, it must react more quickly to disturbances, and it must enable straightforward future upgrades. To achieve these objectives, two different approaches were investigated. These were: first, a PID digital controller to act as a modernized version of the existing analog control system, and second, commercially available load cells placed in line within the pushrods directly connected to the balances. The commercial load cell approach was selected for implementation. This upgrade scheme resulted in an improvement on the accuracy, settling time, reliability, and serviceability of the existing system while eliminating one of its largest sources of hysteresis. Additionally, total reversion to the original analog system is still readily possible on short notice, should a problem with the new system arise.

DEDICATION

This thesis would not have been possible without the support and guidance of Dr. Edward White, whose encouragement and expertise were in equal measures invaluable over the course of this project. I would also like to thank the LSWT staff: Lisa Brown, Doug Kutz, Ric Warren, Zahir Udovicic, and especially John Kochan. Their assistance, each in their own unique fields of expertise, was invaluable in all steps of this project. Finally, I would like to thank my family, especially my parents, Dan and Lea Ann, for their continuous support and encouragement. You have all helped me grow, not just as a student, but as a researcher, an engineer, and as a person. Thank you all so very much.

TABLE OF CONTENTS

Page

ABSTRACT ii

DEDICATION iii

TABLE OF CONTENTS iv

LIST OF FIGURES vi

LIST OF TABLES ix

1. INTRODUCTION 1

    1.1 Background 1
    1.2 Preexisting Balance Description 5
    1.3 Current Issues 8
    1.4 Objectives 10

2. DEVELOPMENT OF POTENTIAL SOLUTIONS 11

    2.1 Digital PID balance 11
    2.2 In-line Load Cells 20

3. CALIBRATION SCHEMES 53

    3.1 Passive schemes 53
    3.2 Active schemes 53
        3.2.1 Single Point Data 53
        3.2.2 Dumbbell Data 56
        3.2.3 Full Calibration 59
    3.3 System Calibration 62

4. RESULTS, CONCLUSIONS, AND FUTURE WORK 63

    4.1 Criteria Review 63
    4.2 System Performance 64
    4.3 System Results 71
    4.4 Future Work 71

BIBLIOGRAPHY 73

APPENDIX A. ENGINEERING DRAWINGS 74

A.1 PID 74
A.2 Pushrod MKI 75
A.3 Pushrod MKII 76
A.4 Pushrod MKIII 77

LIST OF FIGURES

FIGURE Page

1.1 The LSWT external balance system with poise weight balances highlighted in red. For scale, the I beams the converge at the center of the figure are 12.25 inches tall. .. 2

1.2 Lift force mechanical advantage pushrod and lever system 3

1.3 Drag force mechanical advantage pushrod and lever system 3

1.4 Pitch moment mechanical advantage pushrod and lever system (roll is identical)..... 4

1.5 Diagram of a poise weight balance beam 7

1.6 Piose Weight Analog Controller..... 7

1.7 Flexor Pivot of an Analog Balance Beam..... 9

2.1 The Digital PID Test Balance 12

2.2 Arduino System 13

2.3 Wiring Diagram of Arduino System 14

2.4 Linear Encoder 15

2.5 Drive Motor System..... 16

2.6 Balance State of the Poise Balance..... 18

2.7 Commanded RPM of the Drive Motor 18

2.8 Drag Balance Beam With Instrumented Pushrod, MKI Design 22

2.9 Comparison of the Applied and Sensed Loads 23

2.10 Difference Between the Applied and the Sensed Loads..... 23

2.11 Lift pushrod exhibiting buckling at the load cell 25

2.12 Drag Pushrod Brace Installed, MKIb design 25

2.13 Lift Pushrod Brace Installed, MKIb design..... 26

2.14 Pitch Pushrod Brace Installed, MKIb design 26
2.15 Braced Lift Hysteresis 27
2.16 Braced Pitch Hysteresis 27
2.17 Single Point Test for the Braced Pushrods 28
2.18 Labview Code Control Screen 30
2.19 Example Output Text File 30
2.20 The locked balance 31
2.21 Braced and Locked Lift Hysterisis 32
2.22 Braced and Locked Pitch Hysterisis 32
2.23 Single Point Test for the Locked Braced Pushrods 33
2.24 MKII Redesigned Instrumented Pushrod 34
2.25 Pitch Hysterisis for the MKII Pitch Design 35
2.26 Single Point Test for the MKII Pitch Design 36
2.27 MKIII Instrumented Pushrod 38
2.28 MKIII Instrumented Pushrod Adaptor 38
2.29 Loadup of the MKIII Instrumented Pitch Pushrod 39
2.30 Error Between the Applied and Sensed Loads 40
2.31 MKIII lift mounting block 41
2.32 MKIII drag mounting block 42
2.33 MKIII roll mounting block 43
2.34 Final Pitch Loading and Hysteresis 45
2.35 Final Roll Loading and Hysteresis 46
2.36 Final Lift Loading and Hysteresis 47
2.37 Final Drag Loading and Hysteresis 48
2.38 Final Single Point Test 49

2.39 Baseline Noise in the MKIII System 50
2.40 30 min of Constant Load, MKIII design 52
3.1 Single Point Mounting System 54
3.2 Comparison of single point data 55
3.3 Dumbbell Loading in Pitch 56
3.4 Dumbell Loading in Lift 57
3.5 Dumbell Loading in Drag 58
3.6 Stanford Calibration mounting Rig 60
3.7 Stanford Calibration Data 61
3.8 Drag hysteresis from Stanford Calibration 61
4.1 Final Lift Loading and Hysteresis 65
4.2 Final Drag Loading and Hysteresis 66
4.3 Final Roll Loading and Hysteresis 67
4.4 Final Pitch Loading and Hysteresis 68
4.5 Final Single Point Test 69
4.6 30 min of Constant Load 70
A.1 Arduino wireing diagram 74
A.2 MKI sketch 75
A.3 MKII sketch 76
A.4 MKIII drag sketch 77
A.5 MKIII lift sketch 78
A.6 MKIII pitch sketch 79

LIST OF TABLES

TABLE Page

1.1 Thesis Criteria 10

4.1 Thesis Criteria Results 71

1. INTRODUCTION

1.1 Background

Wind tunnels have been the backbone of aerodynamic research for over 100 years. While the ability to perform advanced analysis and simulations have advanced remarkably over that time, the need for wind tunnels has not diminished. Even the most basic of aerodynamic problems require simplifying assumptions when solved analytically. Computational fluid dynamics (CFD) can achieve this with fewer assumptions but is still fundamentally limited by these assumptions. Direct numerical simulation can circumvent this through raw computational power, but is too costly to be practical for the majority of aerodynamic problems, especially engineering problems for which aerodynamic loas are the principle concern. Because of these limitations. The best way to estimate aerodynamic forces is often to simply test the object in a real flow and record the results.

Texas A&M University began construction on the Low Speed Wind Tunnel (LSWT)[1] in the 1940s. The tunnel was upgraded from an open blow-down tunnel to a closed-loop tunnel in the 1950s. An automatic analog force balance was introduced in the 1970s. More recently, the LSWT controls were upgraded from manual and analog to a fully digital system. However, the force balance remained under analog control. For some time this was acceptable. The pyramidal balance that was installed at the tunnel's inception is a remarkable instrument. Using a system of levers, counterbalances, and pushrods, the pyramidal balance isolates the three wind-frame aerodynamic forces (drag, side, and lift) and the three associated moments (roll, pitch, yaw).

The pyramidal balance uses large mechanical advantage on each of these loads, such that every analog poise weight balance beam experiences a standard range of apparent "local" forces, allowing for interchangeability between the analog balances. Figure 1.1 depicts the external balance system, with each of the balance beams highlighted. Figures 1.2, 1.3, and 1.4 illustrate a 2D approximation of the lever arms used to separate the lift, drag, rolling, and pitching forces and moment exerted on the balance. While simplified, these depictions are useful in gaining an under-

[1] Later renamed the Oran W. Nicks Low Speed Wind Tunnel

standing of the mechanics of the external balance. The remaining moment and force components: yaw and sideforce, can be extrapolated from these figures.

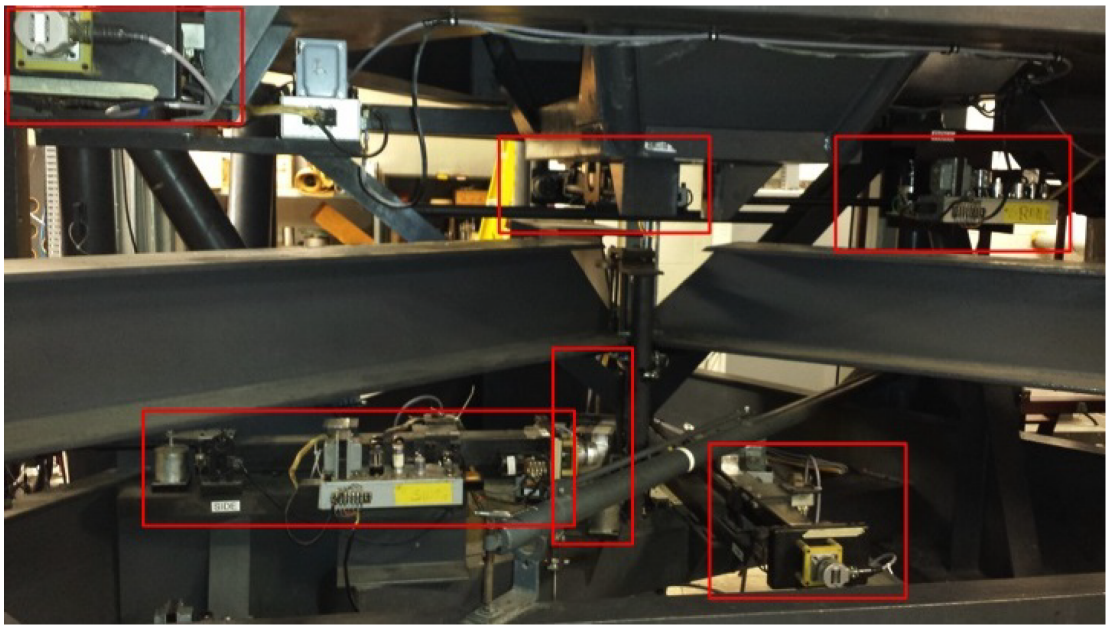

Figure 1.1: The LSWT external balance system with poise weight balances highlighted in red. For scale, the I beams the converge at the center of the figure are 12.25 inches tall.

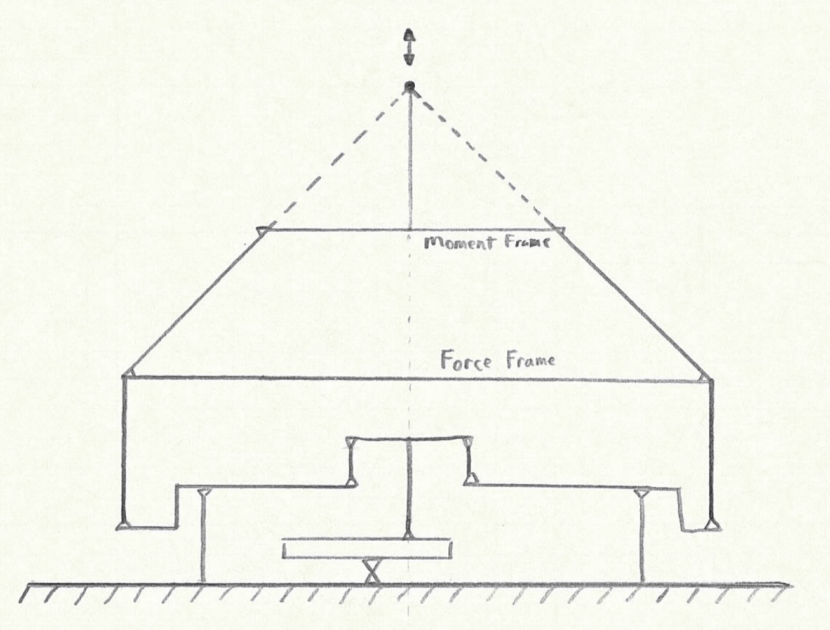

Figure 1.2: Lift force mechanical advantage pushrod and lever system

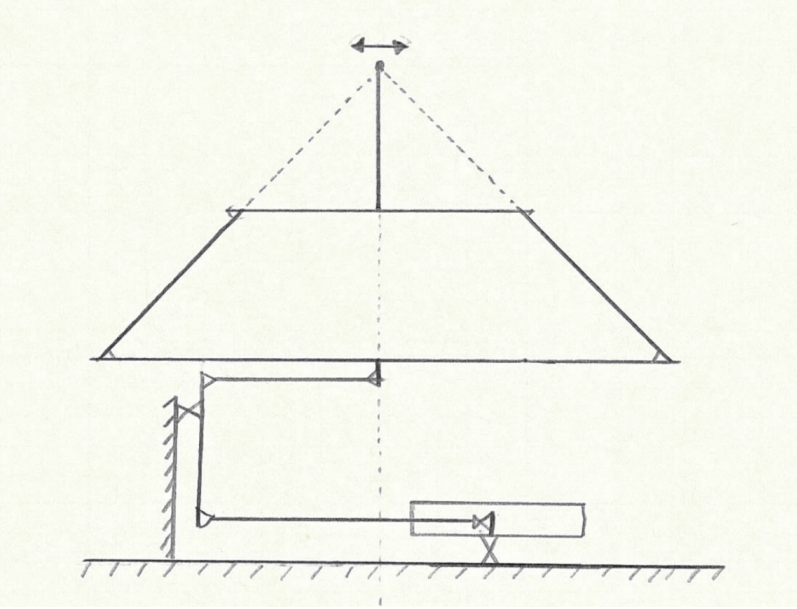

Figure 1.3: Drag force mechanical advantage pushrod and lever system

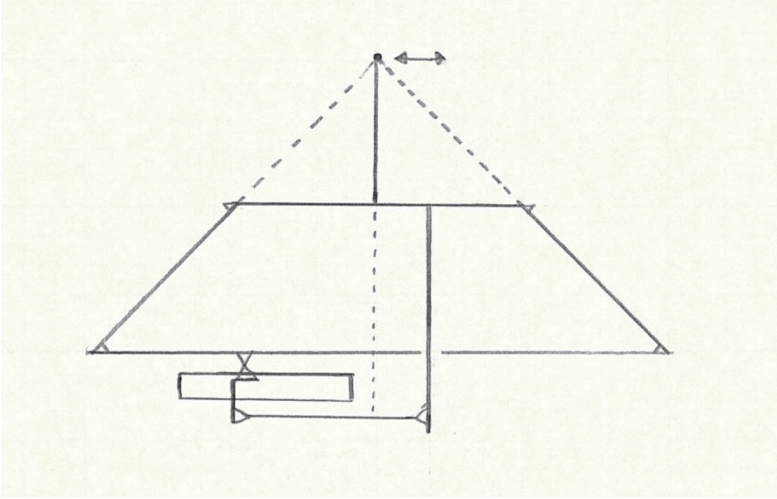

Figure 1.4: Pitch moment mechanical advantage pushrod and lever system (roll is identical)

1.2 Preexisting Balance Description

The LSWT external balance uses six independent balance beams to measure the forces and torques applied to the model. Each of these balance beams operates using the same principle of balancing torques. The input torque is applied by the final pushrod of the pyramidal balance which applies a force at a known distance from a pivot flexor. This torque is balanced by a poise weight varying its position from the pivot flexor. Using this scheme, the magnitude of the applied force can be determined from the position of the weight when the system is in equilibrium. Figure 1.5 presents a diagram of this poise weight balance scheme. To control this system, the balance was controlled by an analog PID system. Deviations from equilibrium are detected by an analog linear potentiometer connected at one end of the balance beam. This sensor detects displacement and changes the return voltage to the controller. The controller then uses an analog PID scheme to drive a double wound electric motor to move the poise weight by turning a lead screw until the balance arm displacement measured by the analog linear potentiometer is minimized and the balance has returned to equilibrium. The position of the weight is determined by a rotary encoder connected to the end of the lead screw. The change of position of the weight is directly related by the angular change in the screw by the threads per inch of the threaded rod. This system is limited by the sensitivity of both the linear potentiomiter and the rotary encoder, as well as the hysteresis associated with a moving balance beam.

This analog balance system has many features that enabled it to remain useful and accurate for decades. First, the sensitivity of the balance is driven by the sensitivity of its two sensors: the analog linear potentiometer and the rotary encoder. The analog linear potentiometer is particularly impressive. Despite its age, the sensitivity of this sensor is equal to or even superior to most high-end digital linear encoders. The rotary encoder is attached to one end of the threaded rod. By recording the number of encoder counts as the lead screw rotates, the position of the weight, and by extension the force or torque applied to the balance can be determined. Because the poise weight masses, the lead screw pitch, and the encoder counts do not vary with time, the system does not drift from its callibration over time. Additionally, the potentiomiter is an error signal which is

read by the analog PID circuit, and is driven to zero by moving the poise weight, rather than the actual load measurement.

As a system, the external balance has an accuracy of 0.2 lbs in lift, drag, and sideforce, and 0.2 ft-lbs in pitch, roll, and yaw moments. The discrete sensitivity of the encoders result in a minimum sensitivity of approximately 0.003 lbs in lift, drag, and sideforce, and 0.006 ft-lbs in pitch, roll, and yaw moment. However, in order to overcome the hysteresis inherent to the poise weight system, large overshoots with long, time consuming settling times must be completed for each data point. This in turn results in the necessity to average one second of continuous data to capture the true loading value among oscillations, as well as a decreased load sensing confidence with dynamic loads.

Despite these challenges, the external balance has the advantage of being dependent upon the large scale physical mechanisms of the pyramidal balance, which grants very strong long-term stability in its calibrations. As long as the physical mechanisms of the external balance remain unchanged, small changes in the much more unreliable analog PID circuit are inconsequential to the overall system. A previous thesis found that the external balance calibration matrix had only slightly changed over the 70 years of continuous LSWT operations. This calibration is also tested daily during every test using the single point test, which is described in detail in section 3.2.1. This test involves applying a known load to the external balance and comparing the resultant reading to the historical value. Doing this confirms that the calibrations are still valid and that all poise weight circuits are properly tuned.

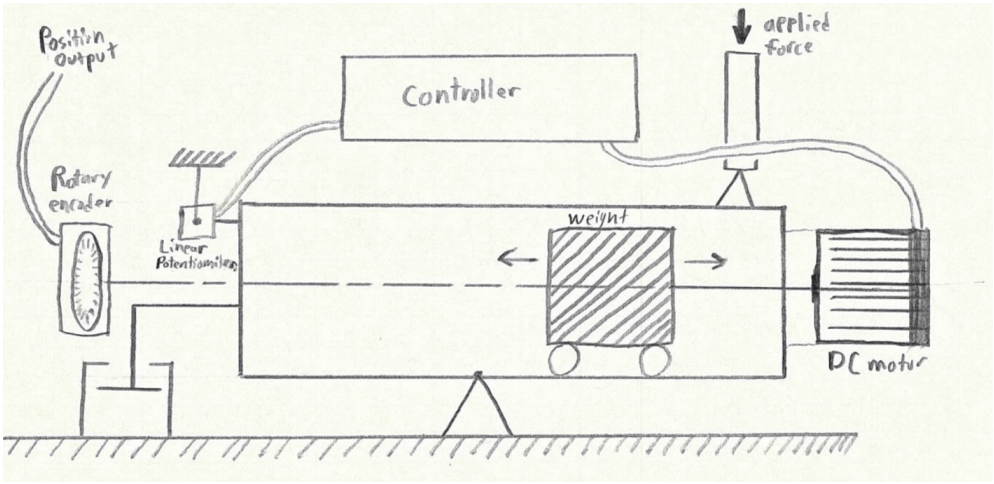

Figure 1.5: Diagram of a poise weight balance beam

Figure 1.6: Piose Weight Analog Controller

1.3 Current Issues

In spite of its advantages that make it such a remarkable system, the old analog balance contains many flaws, both inherent and developed over time. The first issue is the slow reaction times associated with a physical weight driven by a mechanical system. There is considerable lag between a change in model loading and the time required to achieve equilibrium and report a correct load value. Additionally, because the PID system must converge to the new loading state, there are oscillations that must damp before the reported load can be considered correct. This further increases the delay between load and accurate sensor output. These oscillations may be reduced, but cannot be eliminated through PID tuning. They are necessary to overcome a considerable hysteresis effect associated with the flexor pivots, shown in figure 1.7. These flexors, while very low friction, are not hysteresis free. The repeated over and undershoots of the PID scheme are necessary to minimize the hysteresis effect. Because of this, one must either accept lagging readings or hysteresis error.

A second issue with the balance is the long delay before the balance can be used. The vacuum tubes which help control the analog PID control system also require several hours to warm up before they stabilize. This means that the balance must be turned on well in advance of any test.

The drawbacks described above were present when the system was new. Now the analog balance system has begun to exhibit age related problems. For example, it has become increasingly difficult to find replacement parts when vacuum tubes, motors, and bearings fail. Even when replacements can be found, they often perform slightly differently than the originals. This, combined with the general age of the system, has resulted in difficulty in keeping the analog PID variable resistor controls tuned properly. This sometimes results in test delays and suspect data as the balance beams must be constantly monitored and tuned. More pressingly, the transformers powering the balance and the motors driving the lead screw have all degraded with time and have become potential fire hazards.

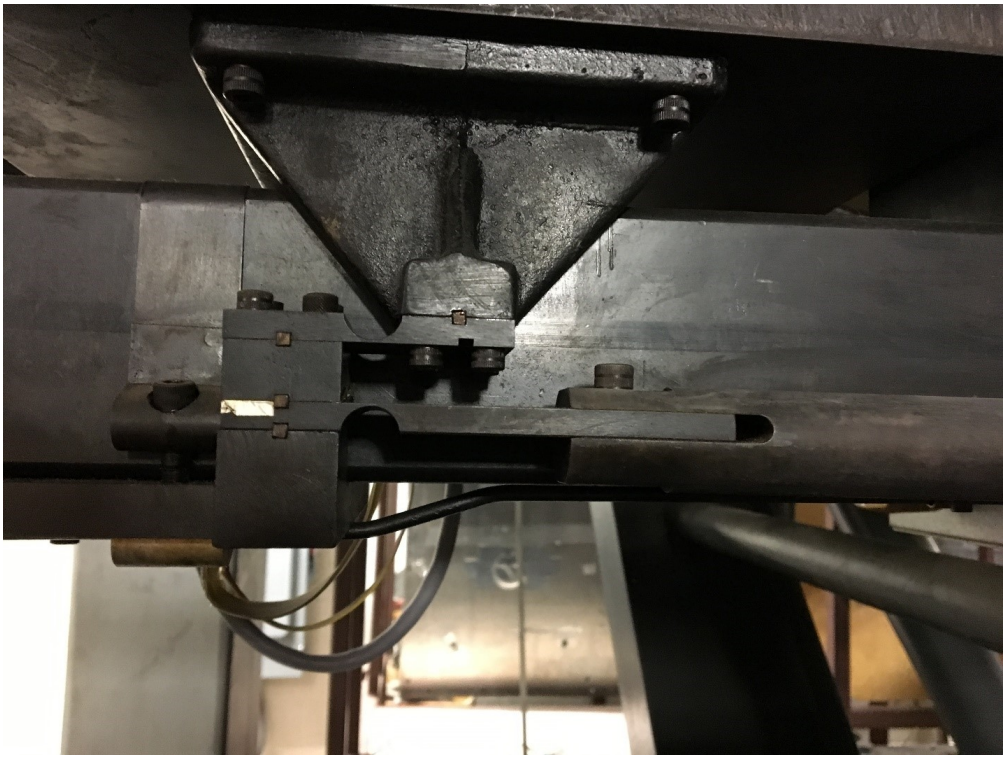

Figure 1.7: Flexor Pivot of an Analog Balance Beam

1.4 Objectives

The goal of this thesis project is to upgrade the LSWT external balance that removes the vacuum-tube driven PID feedback control system. To be considered a success, this upgrade must, at a minimum: match or improve on the accuracy, settling time, reliability, and serviceability of the existing system. The new system should also be able to be implemented with a minimum disturbance to the existing physical balance, and minimize impacts on the testing schedule of the LSWT. Table 1.1 presents the criteria for success in tabular form.

Table 1.1: Thesis Criteria

Quaility	Poiseweight Balance	Thesis Goals
Model Frame Error	0.2 lbs	$\leq$ 0.2 lbs
Reaction Time*	17 seconds	Instantaneous
Hysteresis Rejection	Forced Overshoot	Reduced Overshoot
Data Rate	400 Hz	Variable, 1250 Hz standard
Replacement Ease	Very Difficult	Easy
Reversion Capable	N/A	Yes

* Using Single Point tests as a benchmark

If these criteria can be met, the LSWT will convert the current poise weight balance system over to the new system. To achieve these goals, multiple possible solutions are explored. Results of these efforts are presented in the following sections.

2. DEVELOPMENT OF POTENTIAL SOLUTIONS

Two principal solutions were developed that address the objectives described above. First, a modern digital PID system was explored as an alternative to the analog circuit. This included an updated digital motor and motor controller to drive the poise weight, a digital linear encoder for error positioning, and an Arduino board for PID control. Second, inserting the load cells in line at key points in the pyramidal balance pushrod system was explored as a means of directly measuring the loads being applied to the poise weight balances. Initial development on both systems was conducted in order to ascertain the relative merits of each system. The results of these experiments are described in the following sections.

2.1 Digital PID balance

Initially, the preferred plan was to keep the poise weight system, but upgrade each component with a modern digital system. While this plan seemed to hold promise, problems that arose during development made it clear that the time and effort required to advance the design to a workable state would not be worth the benefits this system would provide.

The first attempted upgrade to the analog balance was to convert it to digital control system. This upgrade would enable the balance's PID controller to be easily tuned through a normal computer interface. Digitally controlled motors could also be driven faster and more precisely to reduce travel and settling times. Finally, the digital components could easily be replaced or upgraded should any be damaged. The digital control programs could also be easily stored and replicated for later repairs or upgrades.

With these potential advantages in mind, proof of concept development was started on this system using a spare balance on a test stand. This unit was retrofitted with a digital readout and voltage supply for an updated encoder. Control was established using an Arduino Uno, which sent servo commands to a commercially available motor controller. This controlled a motor to drive the poise weight lead screw. A digital DC motor, servo, and stepper motor were tested to find

a system with the desired performance. Each of these motors was paired with a corresponding motor controller that translated the Arduino commands to commands that could command by the motor. Each of the motors had similar rated performance but, due to the nature of each motor, each behaved very differently in use. The servo and stepper motors were driven to a commanded position at a commanded speed. This resulted in quick precise motions, but rough, almost piece-wise motion. Conversely, the DC motor was driven only by rotation speed and direction, and therefore had much smoother motion but could not be driven as precisely.

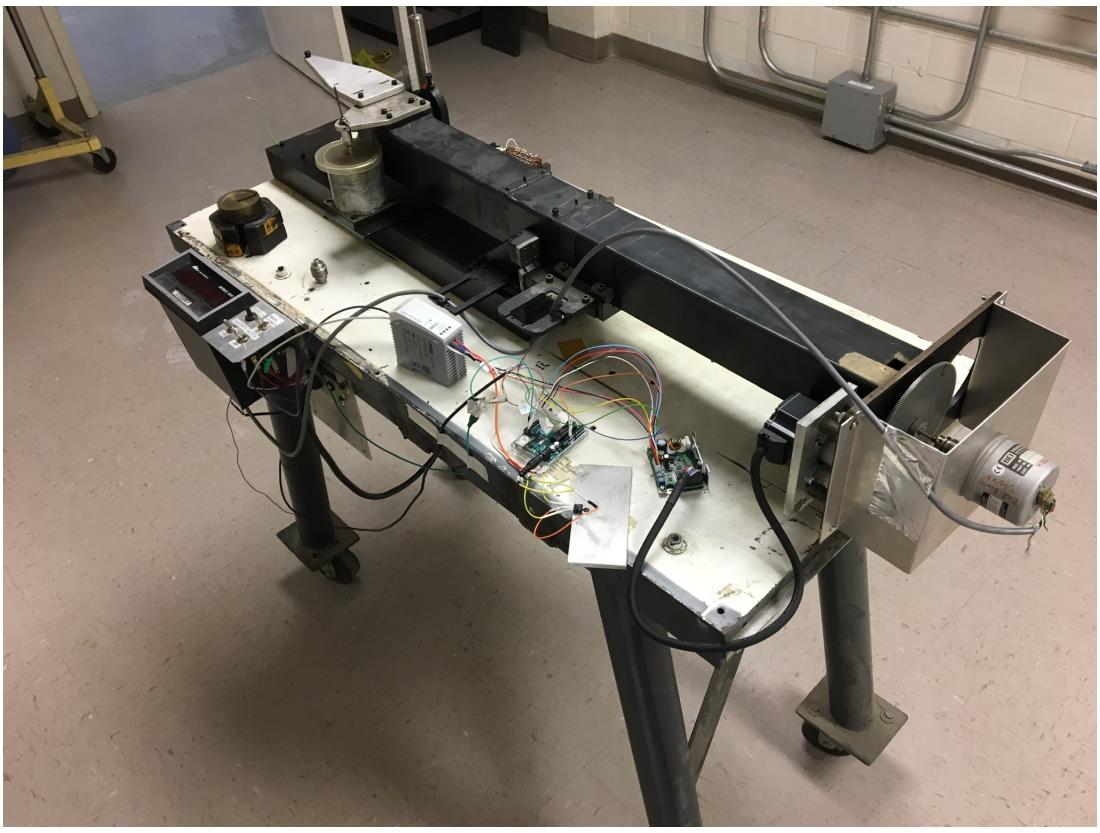

Figure 2.1: The Digital PID Test Balance

Balance beam rotation feedback information was given to the Arduino by a RDP Group 6 inch linear encoder. The H25 incremental optical encoder from BEI Sensors used for this test is identical to those currently in use on the balance beam to record poise weight position[**RDP Group**]. It has

640 counts per revolution, and was rated for speeds up to 12,000 RPM [**Oriental Motor**]. PID control was initially realized using built-in Arduino functions, but were later replaced with custom code developed for this project. The balance was loaded by placing known weights on the balance at known points and observing the whole-system response using a rotary encoder. The code was iteratively refined, with modifications made to the three PID variables (Kp, Ki, Kd), various speed and displacement limitations, as well as to the motor control schemes.

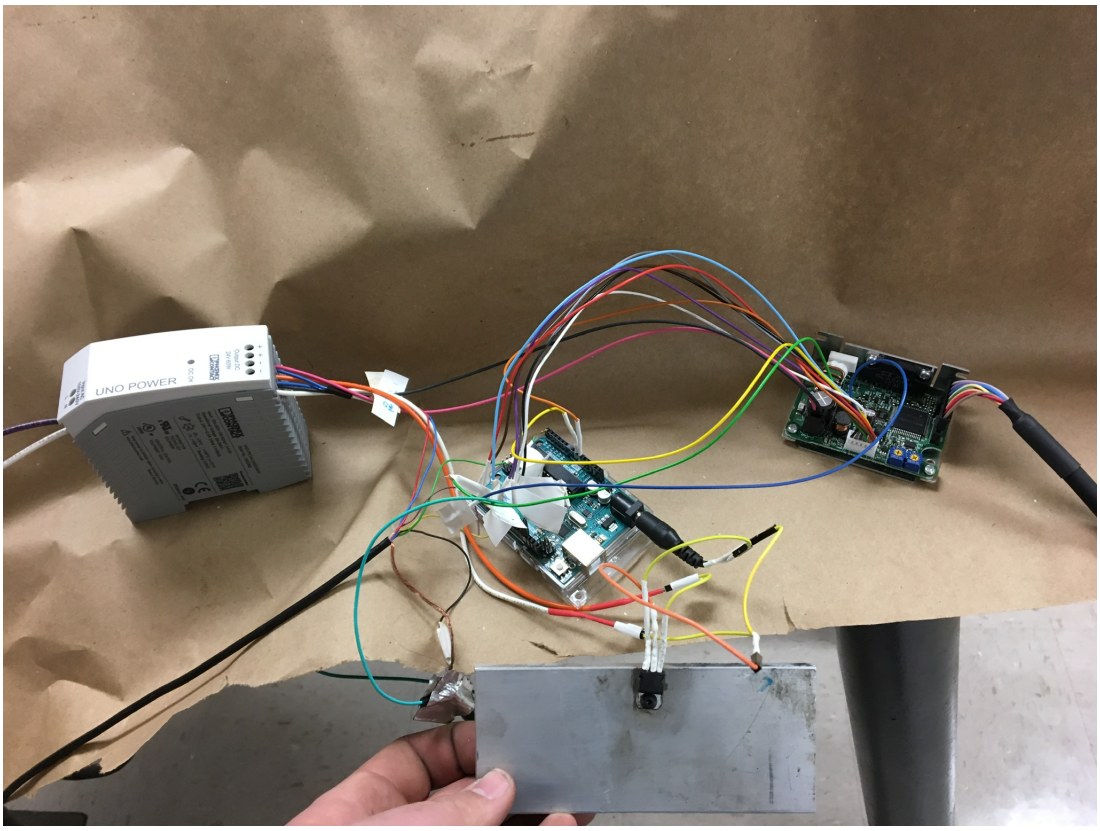

Figure 2.2: Arduino System

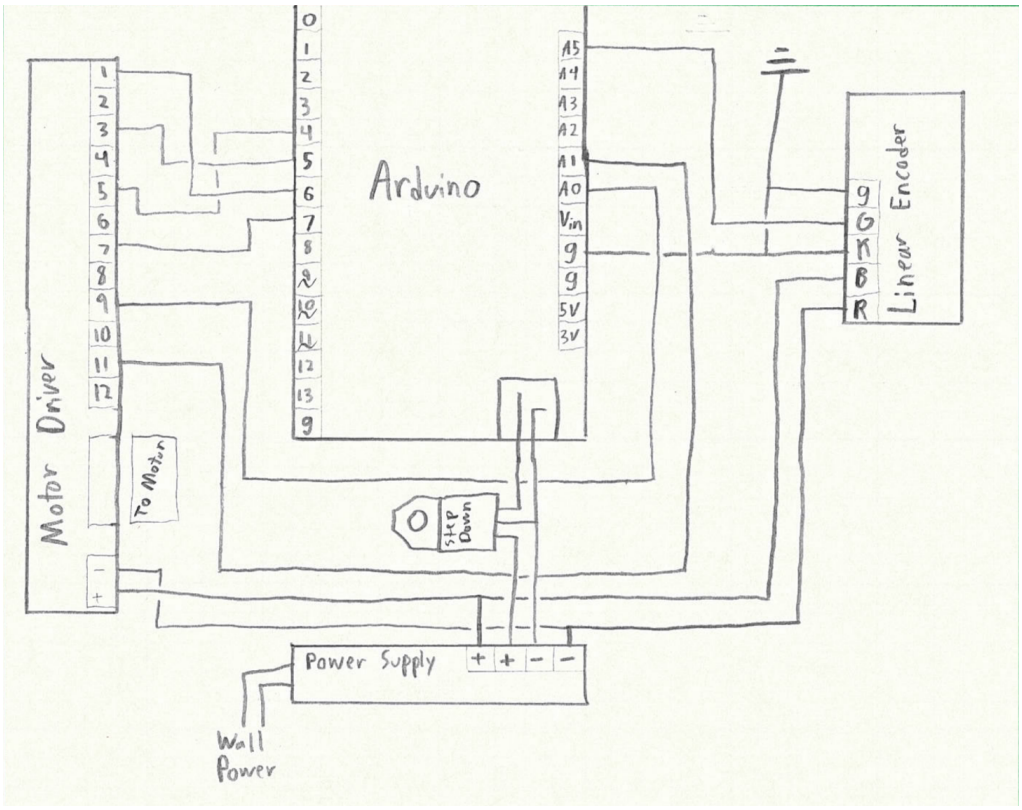

Figure 2.3: Wiring Diagram of Arduino System

Figure 2.4: Linear Encoder

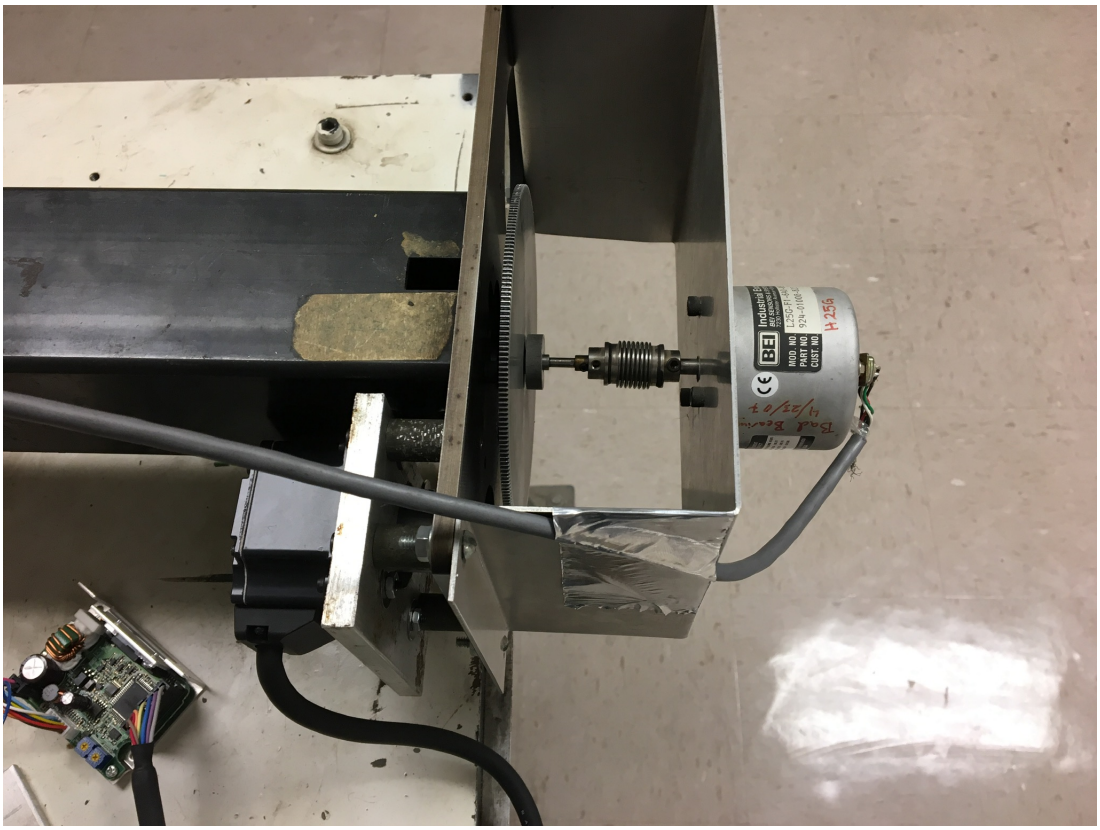

Figure 2.5: Drive Motor System

Ultimately, this approach was abandoned. During testing, it became clear that this scheme provided insufficient advantages over the current system, and substantial flaws were discovered. Firstly, it was determined that the linear encoder used in this setup was inadequate for accurately determining that the balance had achieved its correct equilibrium position. The linear encoder simply did not have the resolution required to accurately and consistently determine the position of the balance. While investigating other potential sensors, it was determined that commercially available digital sensors simply do not have the required resolution. An analog linear potentiometer, wired directly into the analog PID system, has a resolution beyond what is capable for even modern high end digital sensors. Rather than the discrete points of an encoder, a potentiometer uses a combination of electrical resistance and inductance to create an analog signal with exceptionally low error. However, this system cannot easily be replicated in an digital circuit, and therefore is not readily compatible with a digital system. The analog linear potentiometers used on the balance beams had no accuracy limit, due to their design, compared to commercially available encoders which generally report accuracies on the order of 0.03 inches [**RDP Group**].

Additionally, the Arduino is a 10-bit system, which corresponds to a sensitivity of about 5mV [**Arduino**].This sensitivity is worse than the current analog system. Losses encountered in encoder counts, transmission resolution, and digital data encoding all contributed to the propagation of error in the digital system, and these errors fundamentally limited the digital sensors ability to balance the counterweight. By comparison, the analog system and sensor had none of these issues. While a system with greater than 10-bit resolution could have been obtained to address these issues, it would not have resolved all the problems.

The interactions between the motor and the PID controller were also a source of difficulty. The digital nature of the servo and stepper motors and motor controllers mandated that the motors be optimized to be driven to a particular location at constant speed. It would then stop and wait for a new command. However, because the hysteresis associated with the balance's flexors must be overcome, the balance must be slightly under-damped. Taken together, the practical upshot is that the controller must either command the motor in a manner it was designed for, and approach the zero

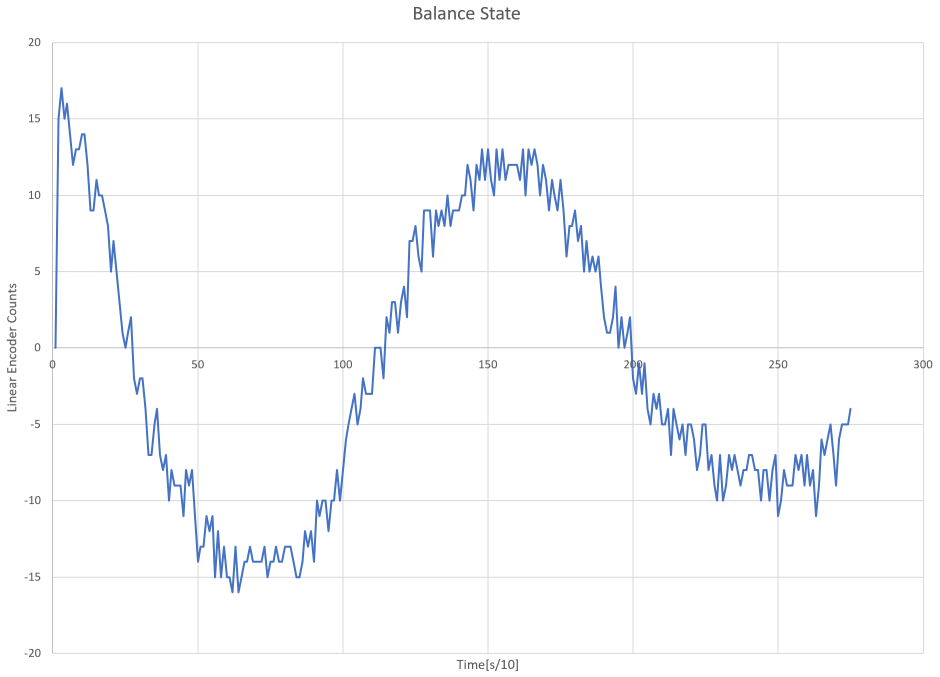

Figure 2.6: Balance State of the Poise Balance

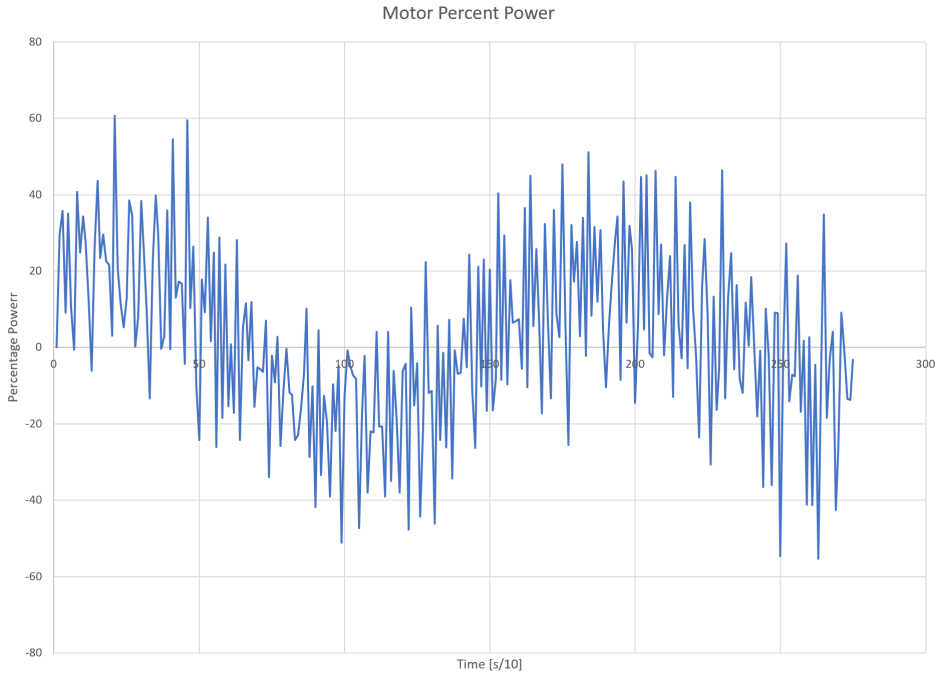

Figure 2.7: Commanded RPM of the Drive Motor

in a discreet step-wise fashion, or the motor must be driven with ever smaller steps, which would allow the balance to much more accurately approach zero, but would quickly overheat the motor. Experiments with continuous control and even decreeing steps sizes resulted in unacceptably high motor temperatures.

The DC motor, due to its smoother operations, exhibited much lower operating temperatures, but the more imprecise nature, combined with the difficulties with establishing balance state, resulted in unacceptably high error, which grew steadily over time.

Figures 2.6 and 2.7 illustrate how, even with the smoother operations of the DC motor, over time the system became more and more erratic. The above plots were generated by placing a weight at a marked position on the balance, and allowing the balance beam to react using the PID system. During testing, dampening initially set extremely high, which would allow the system to be run very conversely. Later, direct limitations to motor RPM were implemented and dampening was reduced to allow for more clear observation of the system response over time. As figure2.7 illustrates, as time increases, the frequency and magnitude of the motor rpm commands steadily increases. This is due not to insufficient dampening, but to the error of the linear potentiometer interacting with the nature of the PID controller. As time goes on, the value of the value of the integral term begins do dominate. However, for a highly dynamic system, like a wind tunnel, this effect must be countered to allow for rapid response to changes in the force applied by the model. Because of this, the stabilizing effect of the integral term is partially lost. This results in a system more vulnerable to disturbances. Coupled with this, the derivative term, even when lowered to below reasonable levels, tended to dominate at longer times, as the system neared the balanced state, the sensor error from the linear potentiometer would trigger the derivative term, and result in the high frequency, increasing amplitude rpm commands that tended to burn up the servo and stepper motors. Additional artificial dampening terms were added, which did slightly improve performance and motor longevity, but came at the cost of much lower motor response times. Additionally, small changes tended to be ignored entirely with the artificial dampening, which, while good for error rejection, meant that small actual changes in load were not detected as well. Ultimately, it was determined

that while continued optimization on the PID code may improve performance, the time and effort required to reach reasonable performance would be better spent investigating other options.

Secondly, while this system would have fully replaced the analog system, it could not have been implemented simultaneously with the analog system, thus making it extremely difficult to revert back to the original analog system. Each balance would have to be completely overhauled with updated controllers, motors, and sensors. This would make it extremely difficult to revert to the original system, should a problem develop with the digital system, and could result in extensive downtime if the problem could not be immediately addressed. For these reasons, it was determined that a digital PID system was not the best way forward for the Texas A&M LSWT.

2.2 In-line Load Cells

The second alternative was to insert load cells into the pushrods ahead of each of the poise weight balance. Doing this would allow for direct digital measurement of the loads being applied to each poise weight balances. Rather than replacing the analog poise weight system with a similar digital system, the poise weights could be bypassed entirely.

Achieving a successful design using the load cells required multiple iterations. The first design, by far the most simple and straightforward, was to simply create a new pushrod with a load cell inserted into it, and is referred to as the Mark 1, or the MKI design. PVC tubing was used to brace the pushrods to counteract bending, and is designated the MKIb design. The MKII design moved the load cell to one extreme end in order to reduce bending. Finally, the MKIII design moved the load cell again and added additional features to reduce bucking, hysteresis, and other factors. The performance of each design steadily improved. Ultimately, the MKIII design was deemed acceptable for use in future LSWT tests.

The first step taken to instrument the pushrods was to calculate the expected loads in each. This was comparatively simple as, thanks to previous investigation with the test balance for the digital controller, both the mass and the total travel of the counterbalance weight are known. Using weight at the maximum position, the maximum load was be determined to be approximately 300 lbs. This value was corroborated by taking the known load limits at the model and performing a

static analysis of the external balance's lever arms to find the force local to the individual pushrods. This method also had the added benefit of giving the scale factor from the pushrod back to the model frame, which is useful during calibration. With the maximum limits of the balance thus determined, the load cells could be properly sized to account for a sufficient factor of safety.

Drag was chosen to be the first balance to be thus instrumented because it has been historically the most accurate of the six balances, according to previous calibrations [**Stanford**]. By having the most accurate balance be the first to be instrumented, any errors made in the manufacture of the instrumented pushrod could be more easily detected by changes in the reported values. Furthermore, this new load cell system could be held to the highest available standard. Additionally, due to the geometry of the pyramidal balance, drag was relatively easy to access, making this and any further modifications substantially easier. This sensor is visible in figure 2.8.

The balance was initially instrumented with a load cell rated for a much larger load, 2000 lbs, which was later reduced to a smaller, more accurate 500 lb load cell once the maximum loading estimates were confirmed. Initial readings taken from these sensors seem to exhibit the expected advantage of speed, because the strain sensor does not need settling time. However, the commercially available load cells also initially appeared to have substantially less accuracy than the old analog balance systems [**Futek**]. While the poise weight could meet the standard 0.2 lb accuracy, the load cell was often several pounds off. However, this error was identified to be stemming not from the load cells, but rather from the DAQ system used for processing their signals. Figures 2.9 and 2.10 illustrate a standard load cycling on the balance using calibrated weights, with both the load cell and analog balance data displayed. This loading method is described in greater detail in section 3.2.

Once the drag poise weight balance was instrumented and initial data taken, lift was chosen to be the next balance to instrument. Compared to drag, lift was much more difficult to access; its lever arm system is substantially more complicated. Lift is also a more average performer amongst the analog balance beam systems and would better serve as a comparison for typical external balance data quality. Data taken from this balance exhibited similar errors to the drag balance.

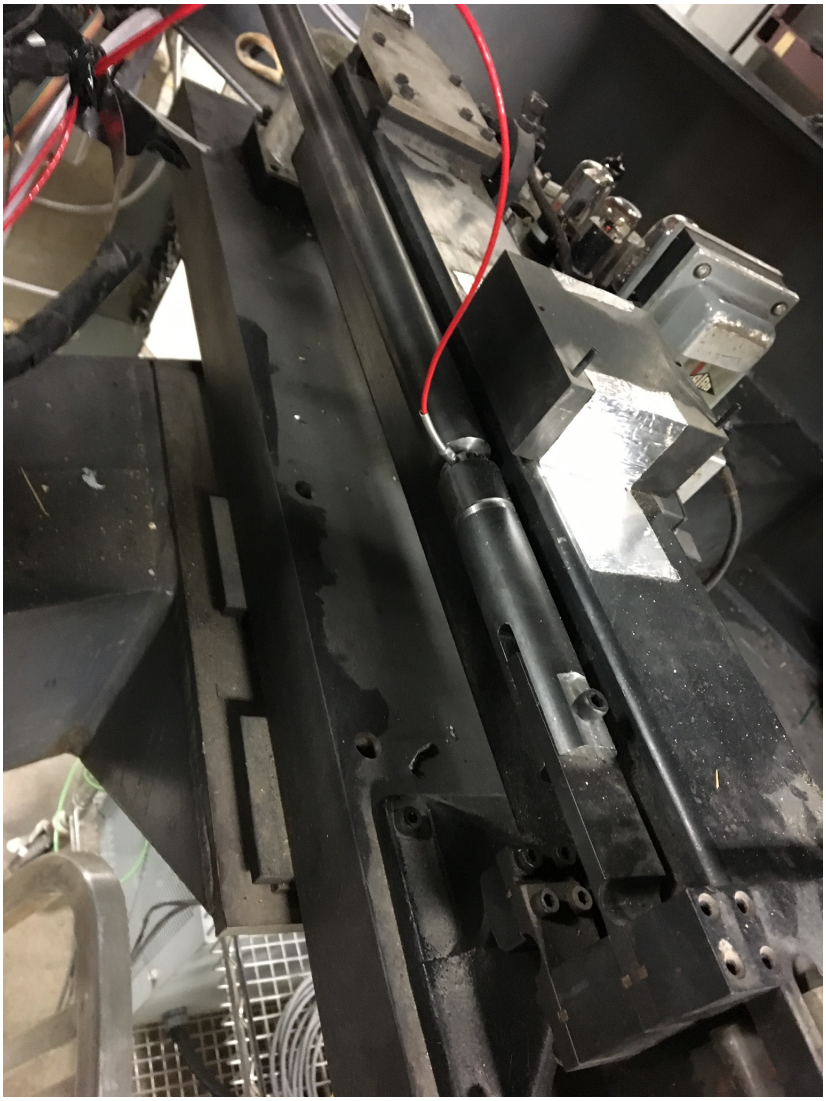

Figure 2.8: Drag Balance Beam With Instrumented Pushrod, MKI Design

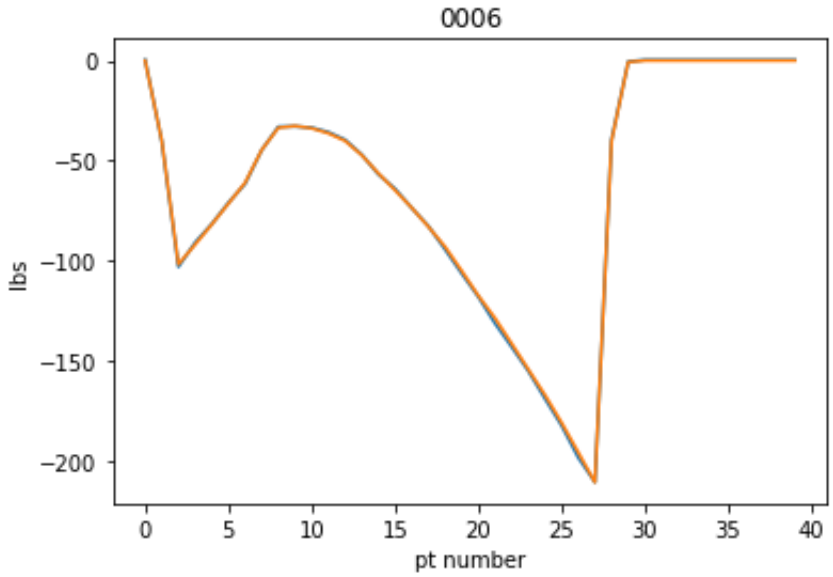

Figure 2.9: Comparison of the Applied and Sensed Loads

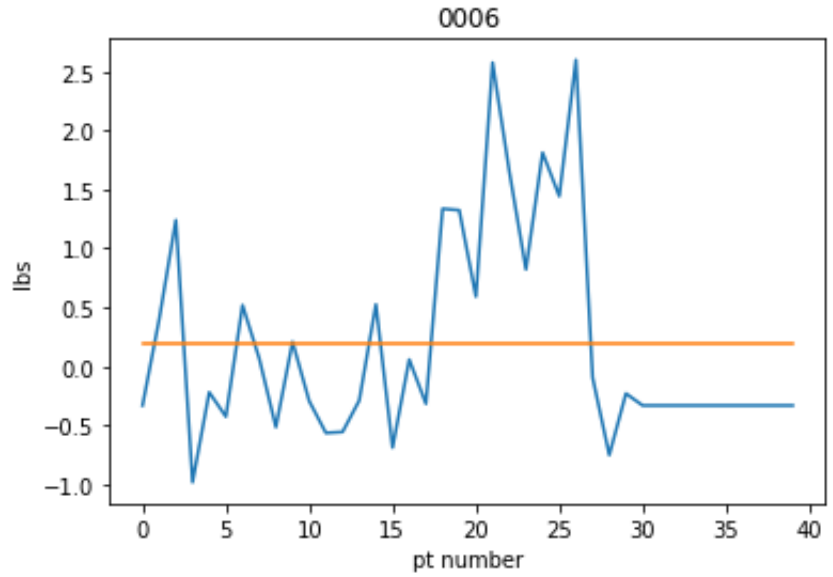

Figure 2.10: Difference Between the Applied and the Sensed Loads

However, it was also observed that the apparent force on the load cell did not scale properly with the force applied. It was theorized that this could be stemming from a bending moment being exerted by the pushrod. Subsequent observations revealed that the pushrod did indeed buckle under the comprehensive load. Figure 2.11 illustrates this bending effect. Essentially, the addition of the load cell introduced a third degree of freedom into the system. The structurally weaker load cell acted as a third flexor and introduced a buckling mode to the system. The load cells were not designed to be tolerant of these bending moments and it is likely that this buckling corrupted the data. This theory was supported by the fact that the error became steadily greater as the force, and therefor the buckling moment, increased.

To eliminate the possibility of buckling, PVC braces were built to sheath around the pushrod. These braces were meant to span to both sides of the load cell, with a channel cut in one side to both allow for the load cell's cabling to exit. The other end of the low friction PVC pipe would be allowed to freely slide on the oiled steel rod. This provided a low friction constraint to resist bending, while allowing axial forces to be freely transmitted to the load cell. This constituted the MKIb design. Minimizing friction reduces hysteresis generated by this alternate load path introduced by the PVC pipe. Figures 2.12, 2.13, and 2.14 depict the three braces installed on the balance. Figures 2.15, 2.16, and 2.17 presents the results of this modification.

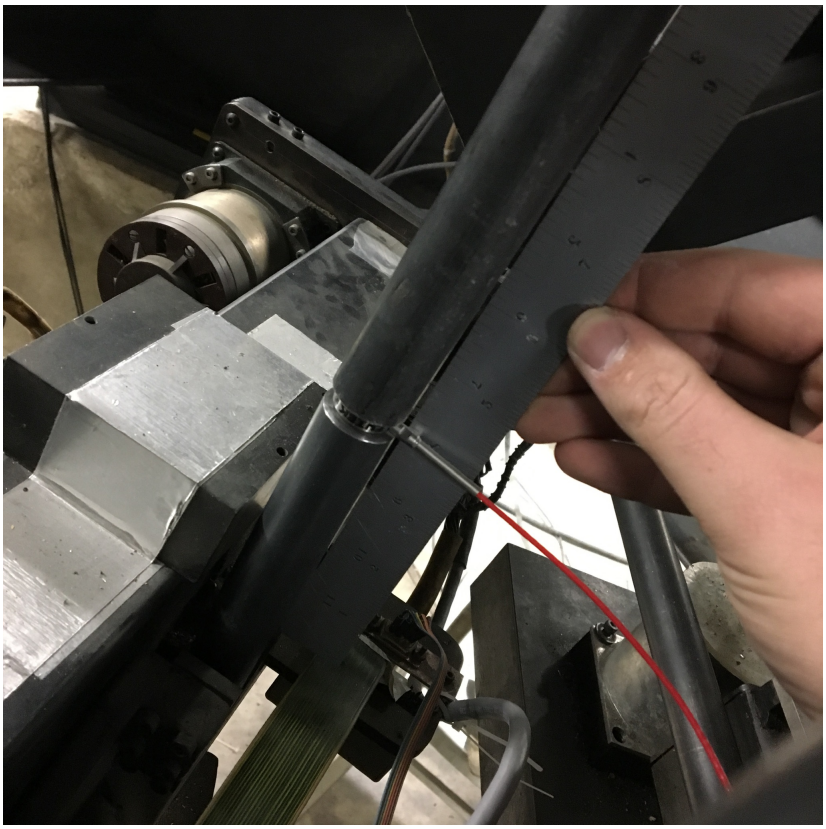

Figure 2.11: Lift pushrod exhibiting buckling at the load cell

Figure 2.12: Drag Pushrod Brace Installed, MKIb design

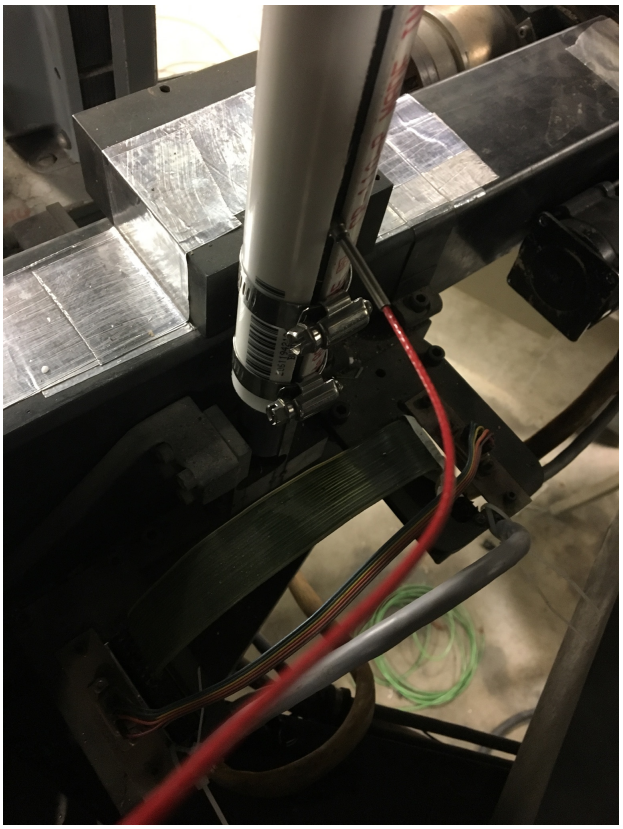

Figure 2.13: Lift Pushrod Brace Installed, MKIb design

Figure 2.14: Pitch Pushrod Brace Installed, MKIb design

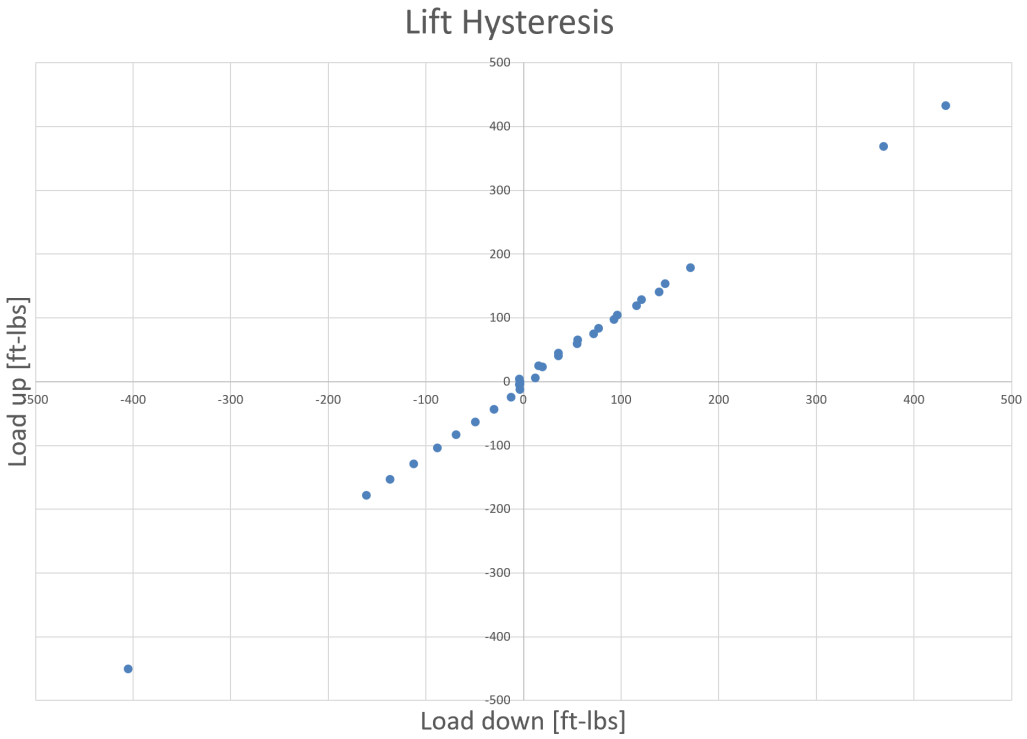

Figure 2.15: Braced Lift Hysteresis

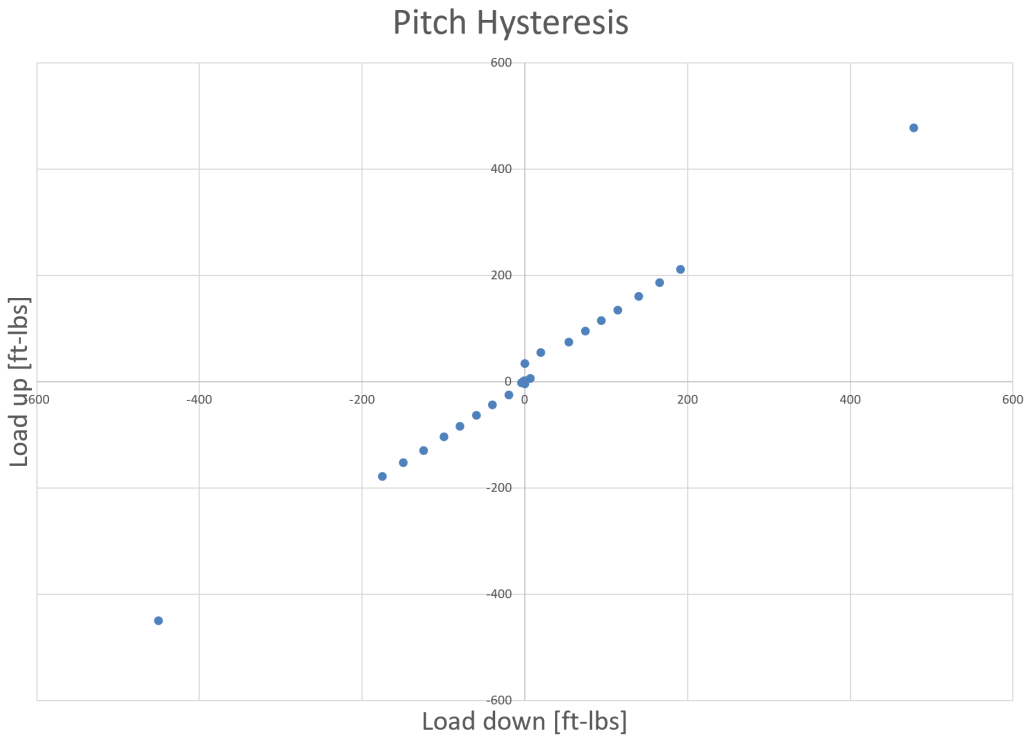

Figure 2.16: Braced Pitch Hysteresis

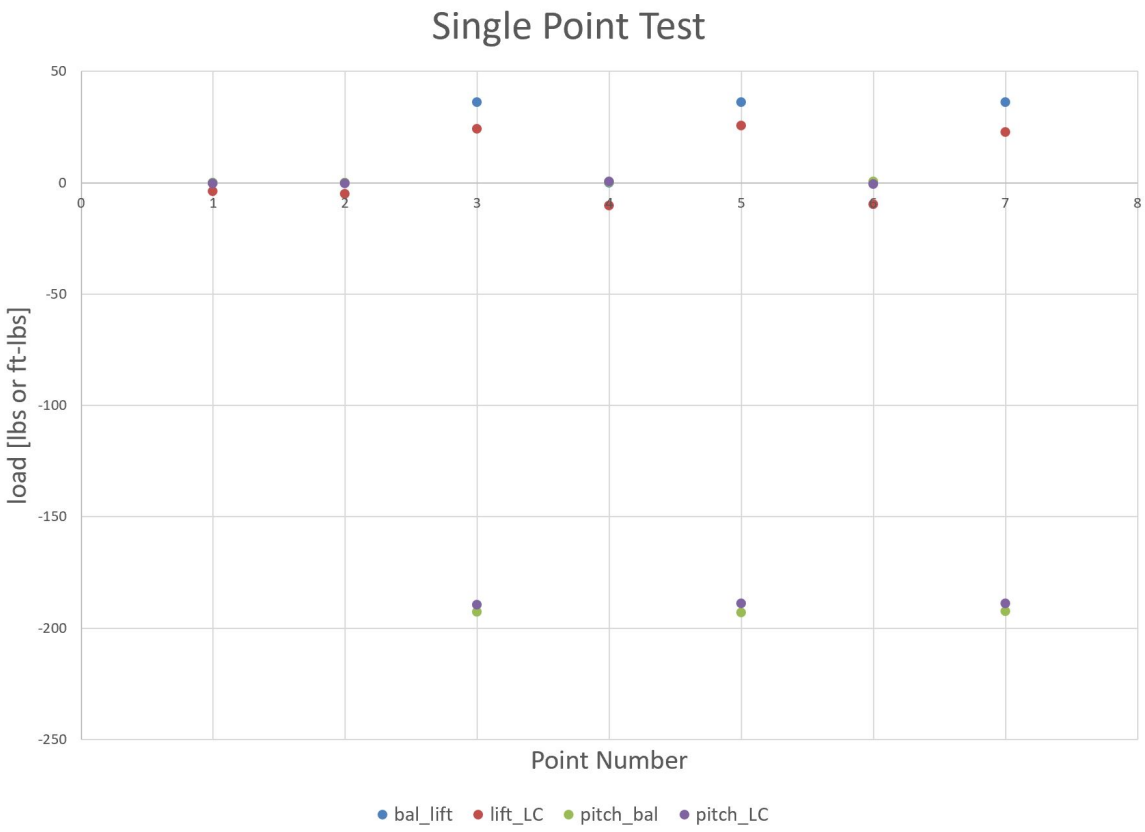

Figure 2.17: Single Point Test for the Braced Pushrods

At the same time the MKIb system was installed, a new DAQ system was also implemented. While the older SCXi DAQ system is used for most standard tests performed at the LSWT, it is insufficient for the needs of this project. For this reason, a new National Instruments PXIe-1071 system was purchased to processes the signals from the load cells. This new PXIe system has nearly 100 times the rated accuracy of the older SCXI, 46.85 mV to 0.4 mV [**National Instruments**]. This enabled much more accurate measurements to be taken from the load cells, and brought the error to within the desired tolerance of 0.2 pounds when the MKIII mounting design was eventually used.

When signals from each load cell are acquired by the PXIe system, these voltage signals are digitized and reported to a computer running National Instruments Labview software. This code receives the voltages from each of the load cells at an arbitrary sample rate, typically 1250 Hz, converts them to forces and moments in the wind frame resolved about the balance mounting center, and then displays and logs this data in one second data samples. This code can also optionally perform data analysis on each one second data packet, obtaining mean, standard deviation, and other statistical values for the one second data set. Output values for each sensor are then compiled and appended into a text document for later analysis. Figure 2.18 is a screenshot of the labview interface, and figure 2.19 is an example text output file.

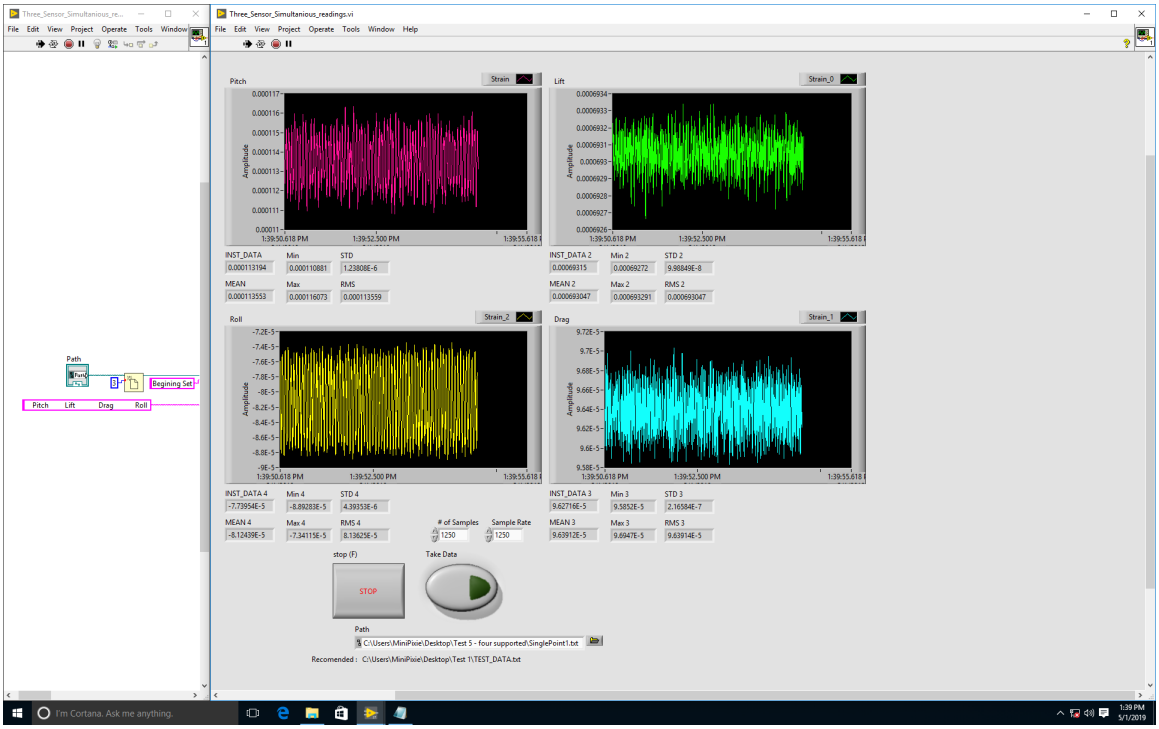

Figure 2.18: Labview Code Control Screen

```
Begining Set
       MEAN                STD                 RMS                 MIN                 MAX      Applied
-0.000105113674700 0.000004778900206 0.000105222198595 -0.000096518397331 -0.000112829804420 0.00
-0.000105145196021 0.000004734820870 0.000105251696260 -0.000097271800041 -0.000113092064857 0.00
-0.000109336265028 0.000005017305350 0.000109451265943 -0.000101147890091 -0.000117306113243 20.00
-0.000109365071952 0.000004976184541 0.000109478166748 -0.000101507902145 -0.000117126107216 20.00
-0.000113504853249 0.000004918526638 0.000113611317743 -0.000105928778648 -0.000121601819992 40.00
-0.000113453311622 0.000005019888803 0.000113564257590 -0.000105747580528 -0.000121315717697 40.00
-0.000117551620007 0.000005094055083 0.000117661887579 -0.000109401345253 -0.000125824809074 60.00
-0.000117551444173 0.000005096049042 0.000117661798210 -0.000109549164772 -0.000125894546509 60.00
-0.000121568637788 0.000005094523226 0.000121675284604 -0.000113372206688 -0.000129582285881 80.00
-0.000121614591777 0.000005120646015 0.000121722293925 -0.000113556385040 -0.000130010843277 80.00
-0.000125552982390 0.000005253606908 0.000125662794702 -0.000116967558861 -0.000133832693100 100.00
-0.000125615563989 0.000005320101944 0.000125728116383 -0.000117110013962 -0.000134213566780 100.00
-0.000130809555054 0.000005194581339 0.000130912603965 -0.000122637152672 -0.000138720870018 125.00
-0.000130746926367 0.000005256712027 0.000130852504597 -0.000122523903847 -0.000138996839523 125.00
-0.000135493912399 0.000005271280313 0.000135596359833 -0.000127191543579 -0.000143635272980 150.00
-0.000135495035946 0.000005331370427 0.000135599830623 -0.000127091407776 -0.000144026279449 150.00
-0.000140668152273 0.000004954169266 0.000140755321693 -0.000132535099983 -0.000148187279701 175.00
-0.000140514648557 0.000005153633420 0.000140609079068 -0.000132653117180 -0.000148624777794 175.00
-0.000198888182044 0.000004493976232 0.000198938921987 -0.000189982652664 -0.000207167863846 200.00
-0.000198987661600 0.000005051898084 0.000199051748002 -0.000187454819679 -0.000209486484528 200.00
-0.000139779486656 0.000004903428793 0.000139865422753 -0.000131443738937 -0.000147714018822 175.00
-0.000139853836596 0.000004822997838 0.000139936933252 -0.000132246017456 -0.000147355794907 175.00
-0.000135380254984 0.000004822995045 0.000135466095722 -0.000127573609352 -0.000143006443977 150.00
-0.000135347547233 0.000005012668093 0.000135440292454 -0.000127468705177 -0.000143147706985 150.00
-0.000130565732419 0.000004236571280 0.000130634413706 -0.000123737454414 -0.000137398838997 125.00
-0.000130487940311 0.000003883678849 0.000130545693099 -0.000123599767685 -0.000137724280357 125.00
-0.000125474346578 0.000004564410354 0.000125557297973 -0.000118065476418 -0.000133031606674 100.00
-0.000125515585244 0.000004570986935 0.000125598748456 -0.000117821693420 -0.000133074522018 100.00
-0.000121482349038 0.000005222576478 0.000121594501501 -0.000113604664803 -0.000129773020744 80.00
-0.000121519396901 0.000005163810009 0.000121629007332 -0.000113449692726 -0.000129430890083 80.00
-0.000117336714268 0.000004952927910 0.000117441150132 -0.000109345912933 -0.000124992132187 60.00
-0.000117256773412 0.000005060035557 0.000117365847114 -0.000109402537346 -0.000125505328178 60.00
-0.000113261007667 0.000004849952453 0.000113364748204 -0.000105385780334 -0.000120935440063 40.00
-0.000113222878277 0.000004904632045 0.000113329005789 -0.000105726718903 -0.000120692849159 40.00
-0.000109226373136 0.000004850938801 0.000109333985704 -0.000101653933525 -0.000116753578186 20.00
-0.000109209058285 0.000004786691693 0.000109313857185 -0.000101757645607 -0.000116642713547 20.00
-0.000105136078298 0.000004886230047 0.000105249504827 -0.000097268223763 -0.000112838149071 0.00
-0.000105116709471 0.000004886064629 0.000105230149200 -0.000097526311874 -0.000112539529800 0.00
-0.000105021351278 0.000004834348289 0.000105132504308 -0.000097401738167 -0.000112993717194 0.00
```

Figure 2.19: Example Output Text File

The data from the MKIb braced design indicates that buckling in the pushrods was indeed the source of the nonlinear error in the load cells. However, significant hysteresis was also incurred by bracing the load cells using PVC pipe. For this reason, the decision was made to redesign the instrumented pushrods such that no bracing would be required to resist buckling. This would remove the need for the bracing, and the hysteresis they cause.

During data acquisition for the braced test, another potential source of error was identified. Because of the oscillations of the balance, the local force applied to the load cells was not constant, but was related to the balance state of each of the poise weights. To test this, all balances were locked and deactivated before using the same set of known weights to load the balance. This process and its results are displayed in figures 2.20 through 2.23.

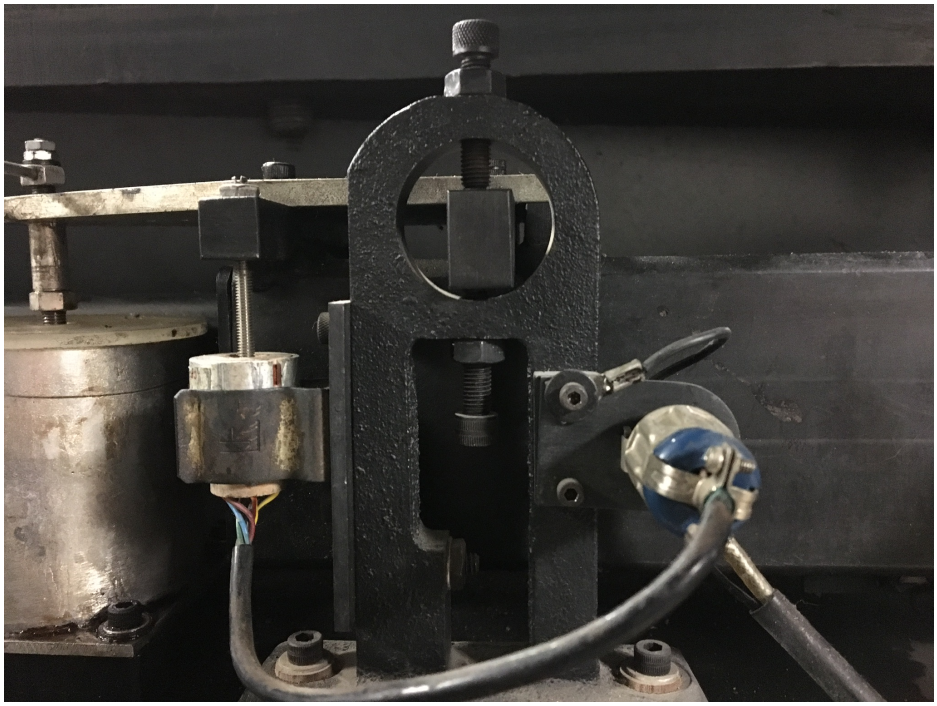

Figure 2.20: The locked balance

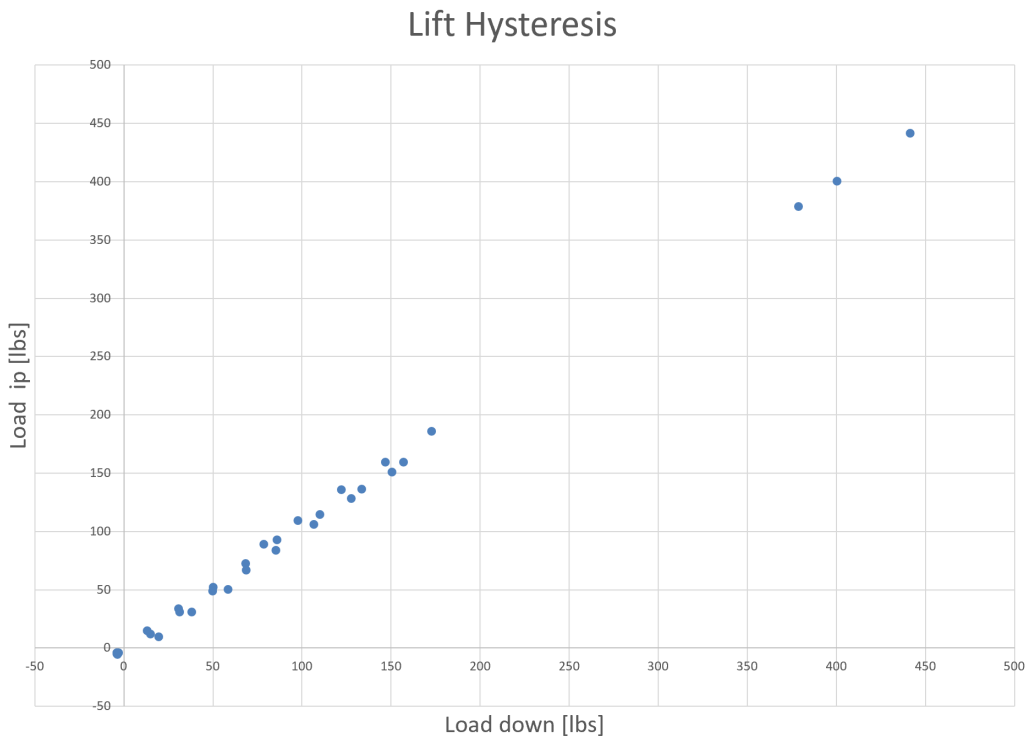

Figure 2.21: Braced and Locked Lift Hysterisis

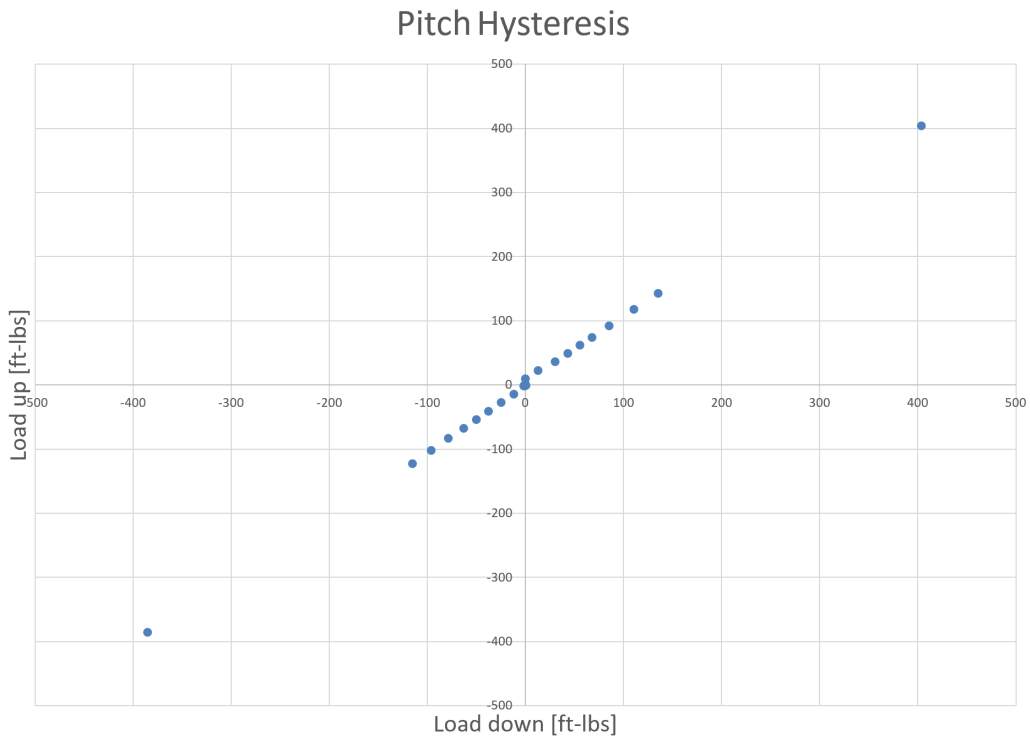

Figure 2.22: Braced and Locked Pitch Hysterisis

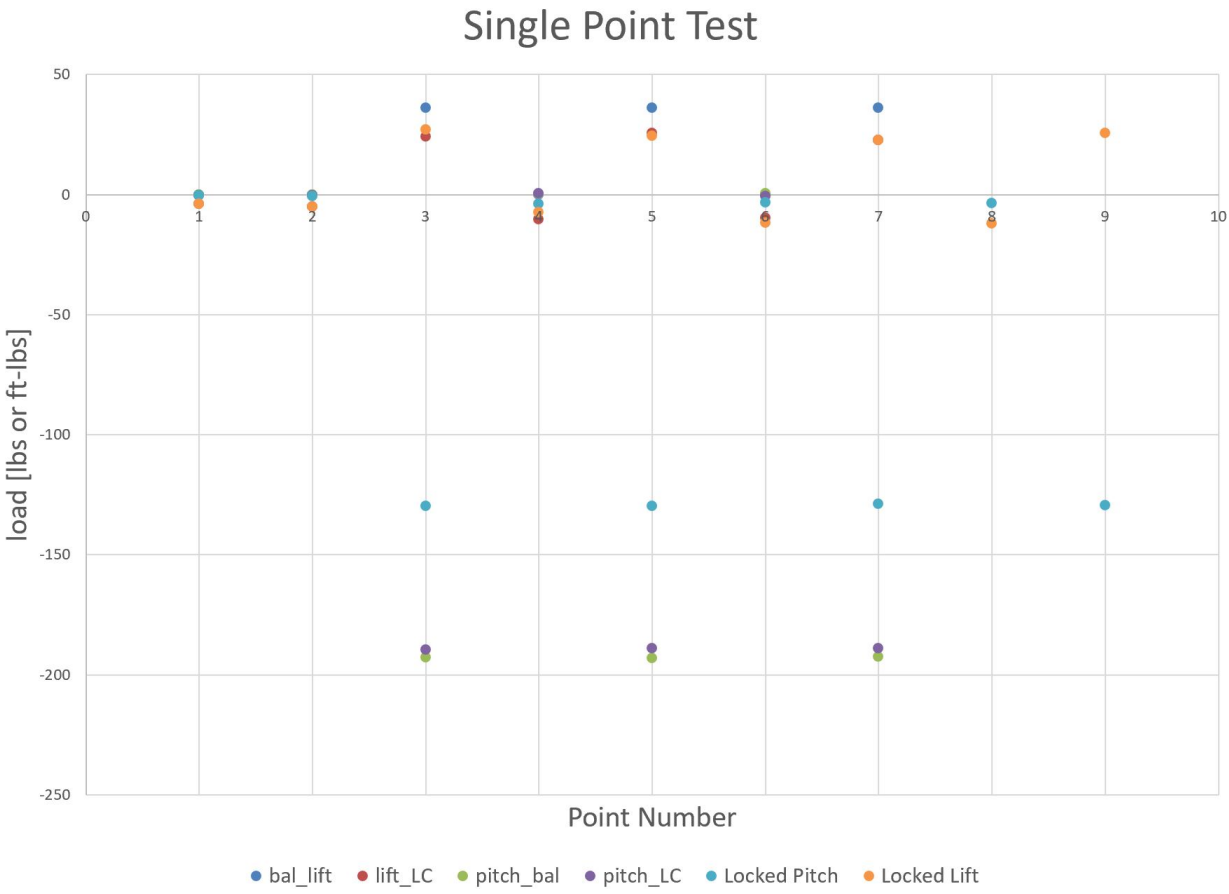

Figure 2.23: Single Point Test for the Locked Braced Pushrods

In order to reduce the opportunities for buckling to occur, while simultaneously helping to remove hysteresis associated with both bracing and flexors, the strain gauges were moved from their previous location just ahead of the poise weight flexor to the extreme other end of the pushrod. More specifically, the load cell replaced the flexor cube on each of the pushrods. This configuration is illustrated in figure 2.24.

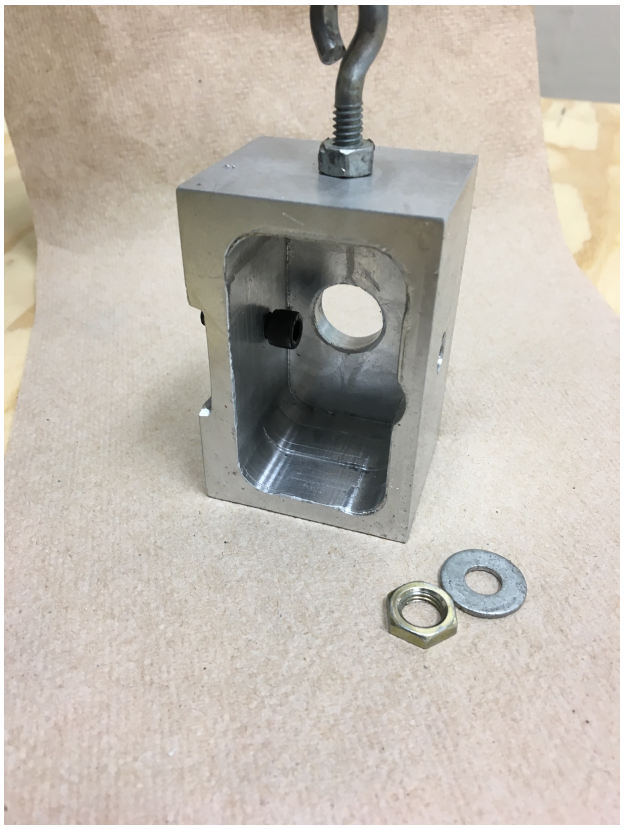

Figure 2.24: MKII Redesigned Instrumented Pushrod

Figure 2.24 also highlights the adapter block that allowed the load cell to be placed directly against the balance saddle.

This iteration of the design was successful in eliminating the rod bending, as expected of removing a degree of freedom from a system. However, the hysteresis appeared unchanged. Figure 2.25 illustrates the reduction of non-linearity, but no perceptible change in the hysteresis of the

system. Additionally, during the course of the testing, it was noted that the roll poise weight balance was extremely sensitive to small offsets in the position of the lift pushrod. For this reason, additional care needed to be taken when aligned the pushrod for subsequent tests.

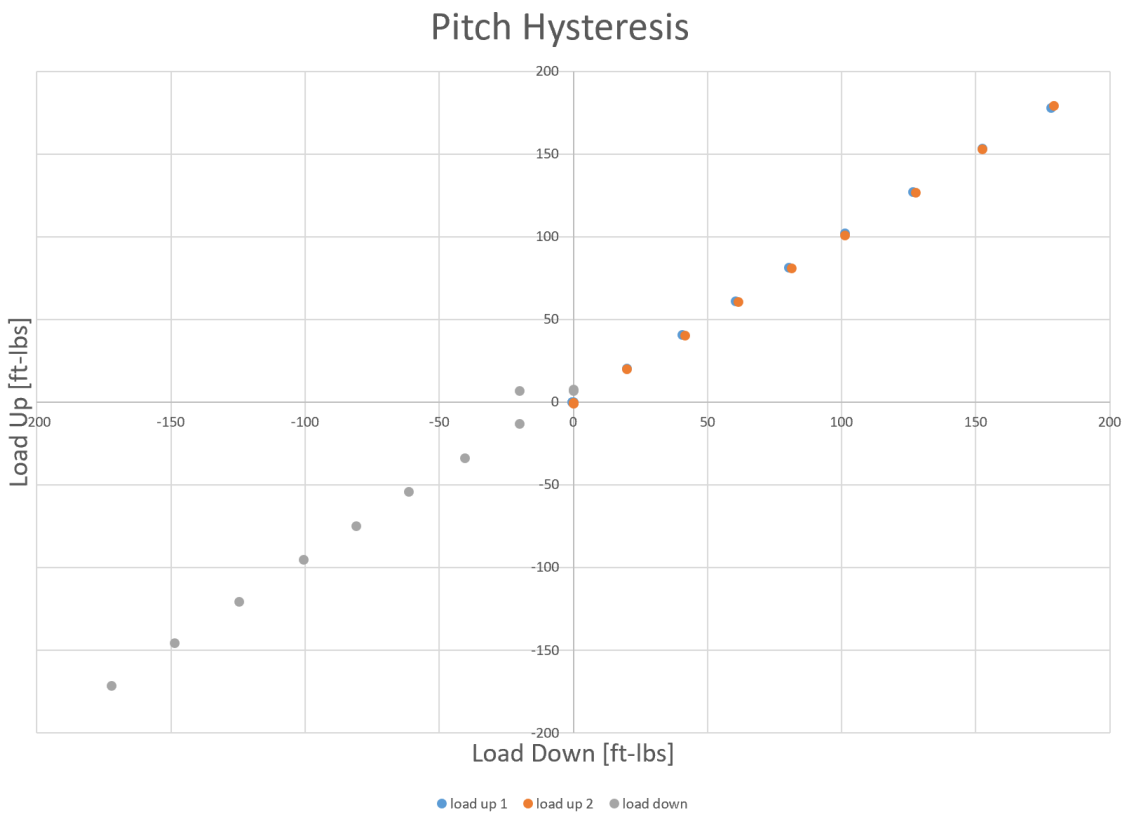

Figure 2.25: Pitch Hysterisis for the MKII Pitch Design

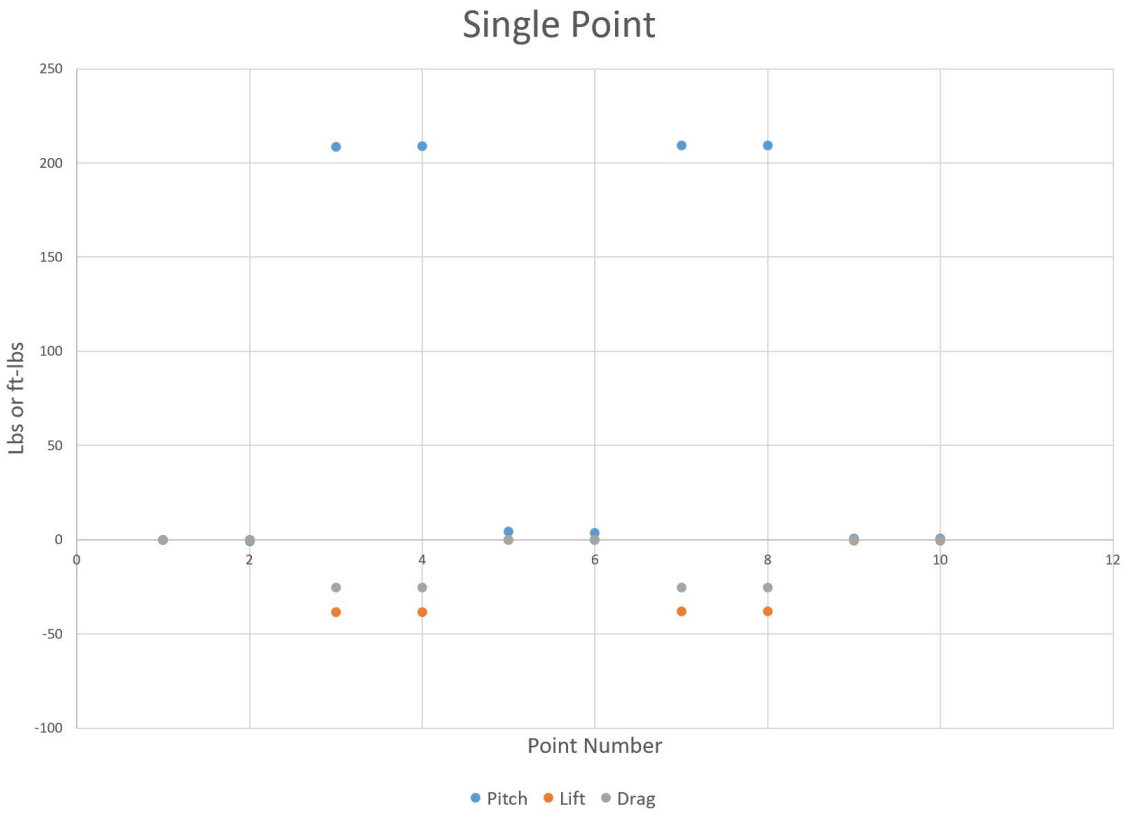

Figure 2.26: Single Point Test for the MKII Pitch Design

A potential source of non-linearity was identified as the weight of the pushrod exerting sideload on the load cell. According to the listed product specifications, each of the load cells can reject some side loading, however, for best performance these loads should be kept to a minimum. To address this issue, an updated adapter design, called the MKIII for clarification, was developed with a suport arm that would brace the pushrod on both sides of the loadcell, illustrated in figures 2.27 and **??**. One end of the load cell is threaded directly into the adapter, which is then bolted to the balance frame. The other end is threaded into the existing steel pushrod, which is supported by the under-hanging arm of the adapter. This arm is equipped with ball bearings with adjustable height to allow for a low-cross-loading, low-friction fit. This design should carry the advantages of previous iterations. Specifically, of being fixed to the frame, which eliminates the hysteresis and feedback of the poise weight; of being "downstream" of the flexor cube, which allows for increased tolerance for slight shifts in the external balance's leverarms; and of mounting the load cell against a fixed body, which reduces buckling. Additionally, the addition of the support arm reduces sideload on the unidirectional loadcell. This MKIII design was tested using the same loadup series for comparison to previous iterations. The results of the loadup tests are detailed below in figures 2.29 and 2.30

One drawback to this design is that with the poise weight balances removed from the system, it becomes difficult to verify the moments being applied to the balance. For this reason, the discrepancies observed in figure 2.29 is not concerning, as the slope offset from the expected 1:1 slope can be attributed to an error of less than 1/4 inch in the hand placement of the applied weights in the model frame. More importantly, it can be inferred from these results that the hysteresis of this system has been reduced to below 0.2 lbs or 0.2 ft-lbs for the forces and moments, respectively, which meets the original standard of less than or equal to 0.2 lbs or 0.2 ft-lbs .

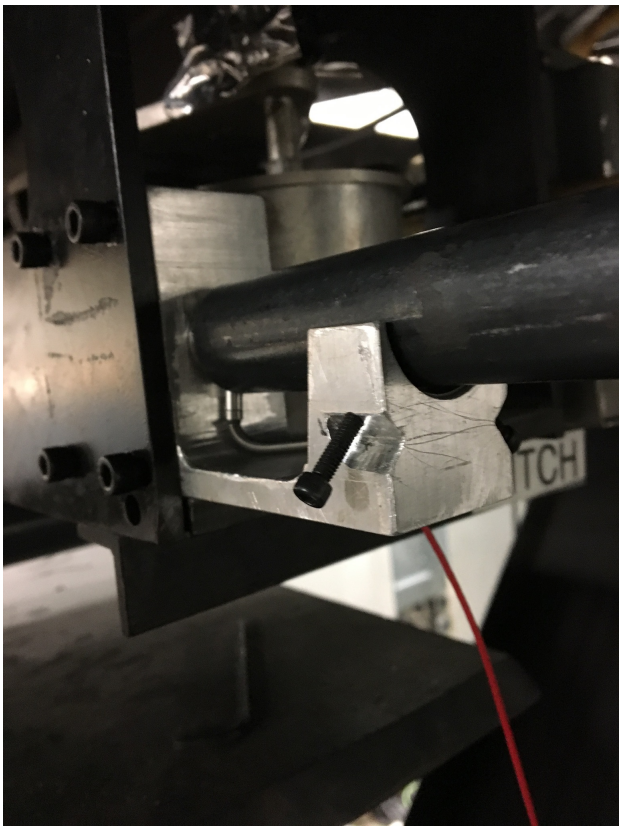

Figure 2.27: MKIII Instrumented Pushrod

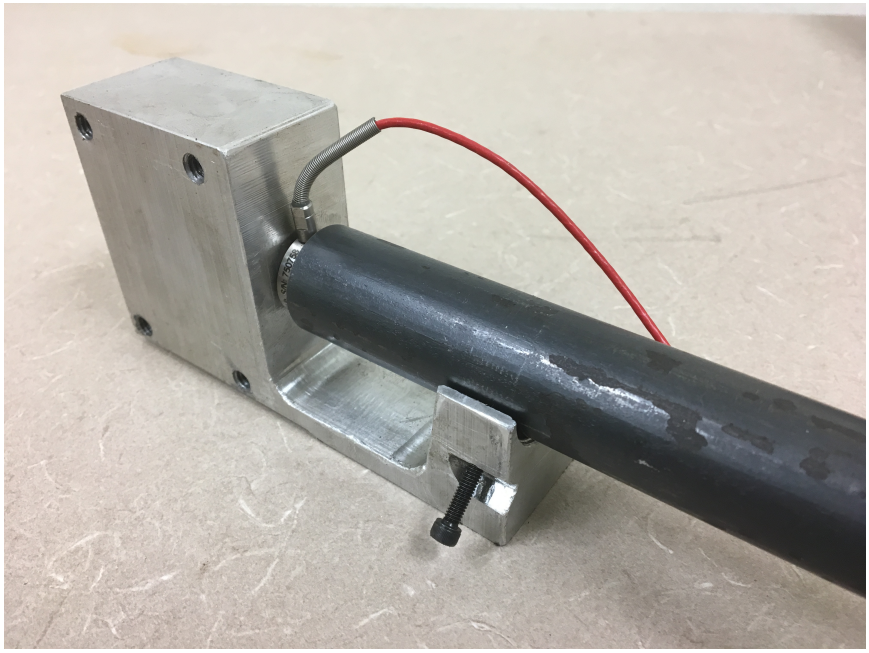

Figure 2.28: MKIII Instrumented Pushrod Adaptor

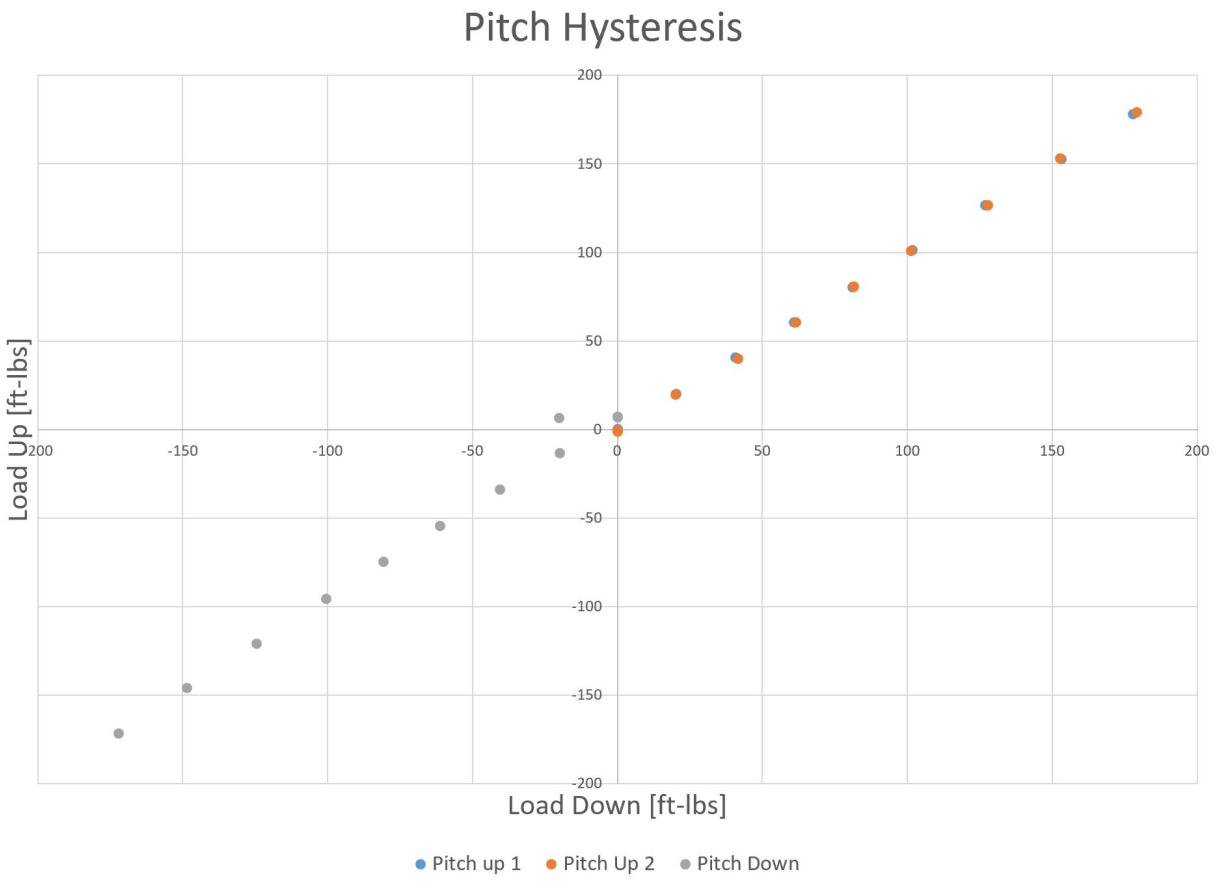

Figure 2.29: Loadup of the MKIII Instrumented Pitch Pushrod

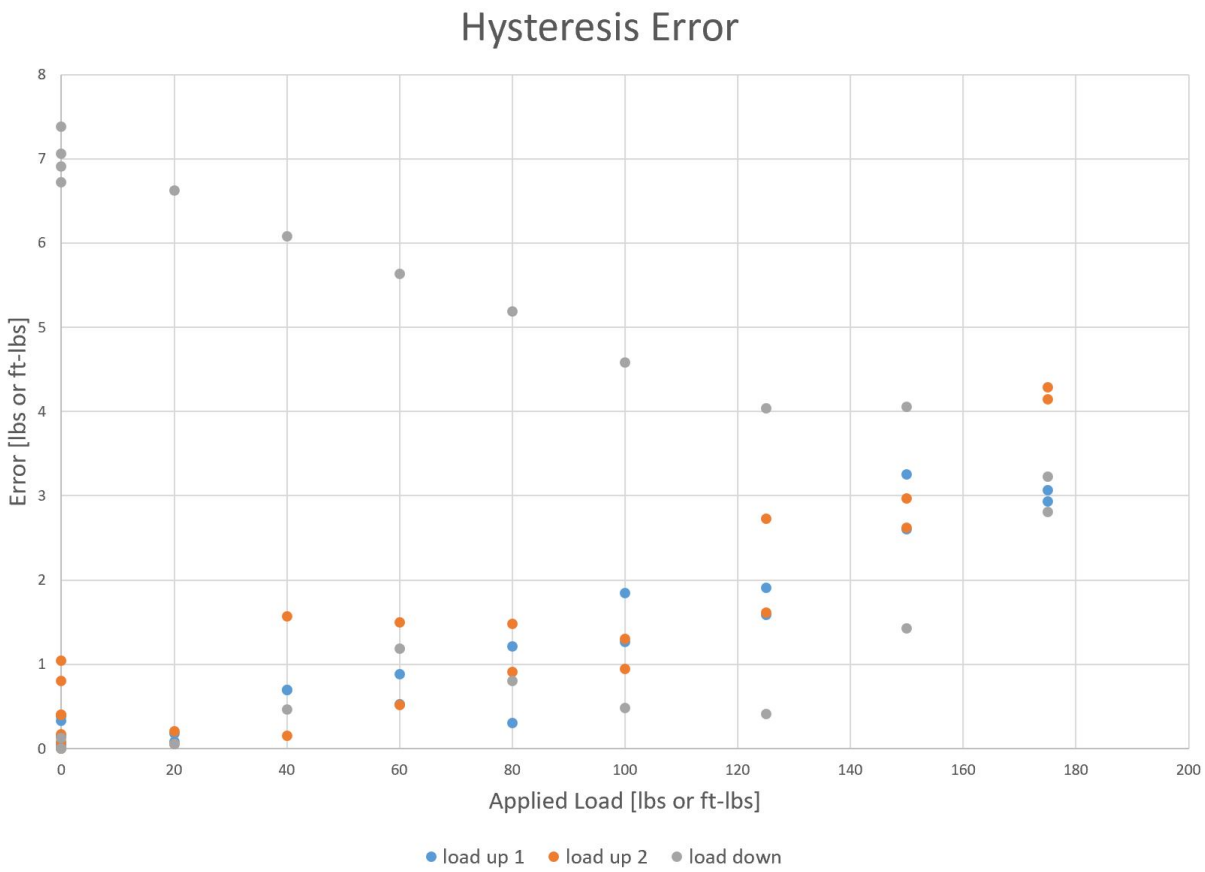

Figure 2.30: Error Between the Applied and Sensed Loads

After the design for pitch was finalized, similar mounting blocks for lift, drag, and roll were machined. These blocks, figures 2.31, 2.32, and 2.33, used similar principles to the MKIII block for pitch, but were adapted to fit the differing mounting locations and directions for each location. Unlike the MKIII pitch mounting block, the MKIII drag, lift, and roll blocks were fixed in place using clamps. This was done deliberately, as each of these blocks was designed to have two faces that would mate to existing surfaces on the balance, so locating the correct position would be simple, and the use of clamps would save much time not only in installation and removal, but also in initial build time. Examination of the distance between the mounting blocks and fixed structures indicated that the blocks did not shift over the course of the test.

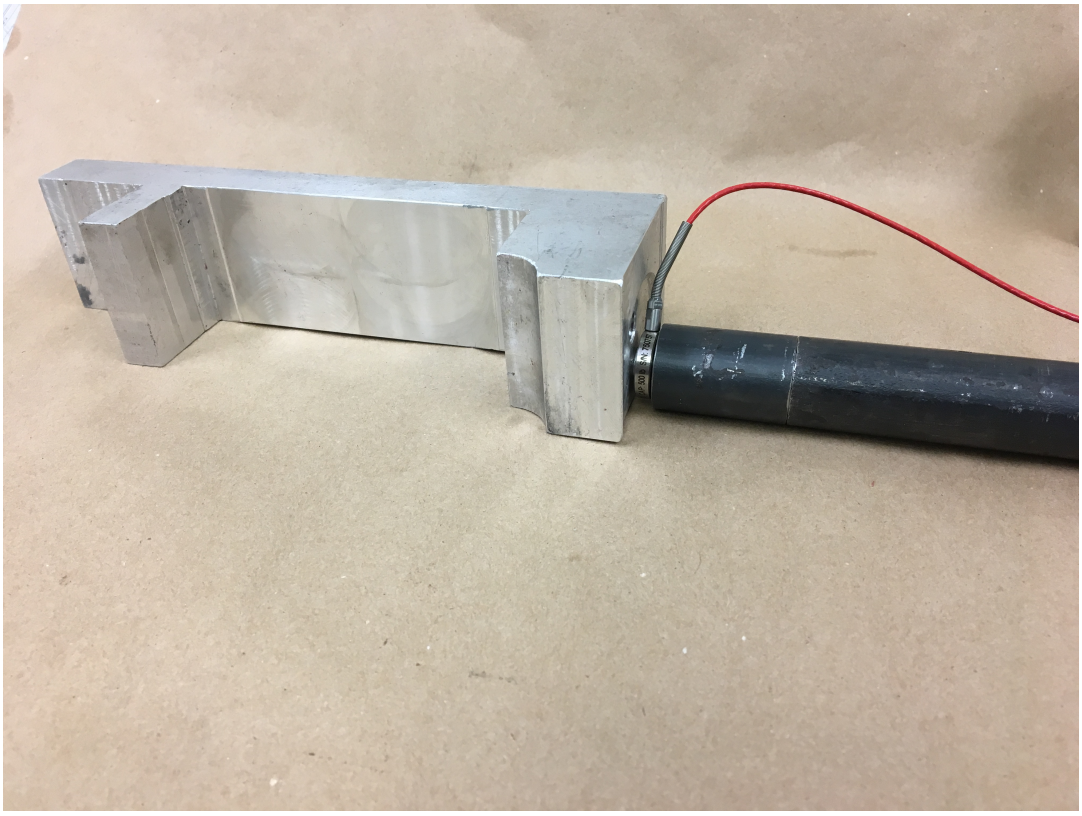

Figure 2.31: MKIII lift mounting block

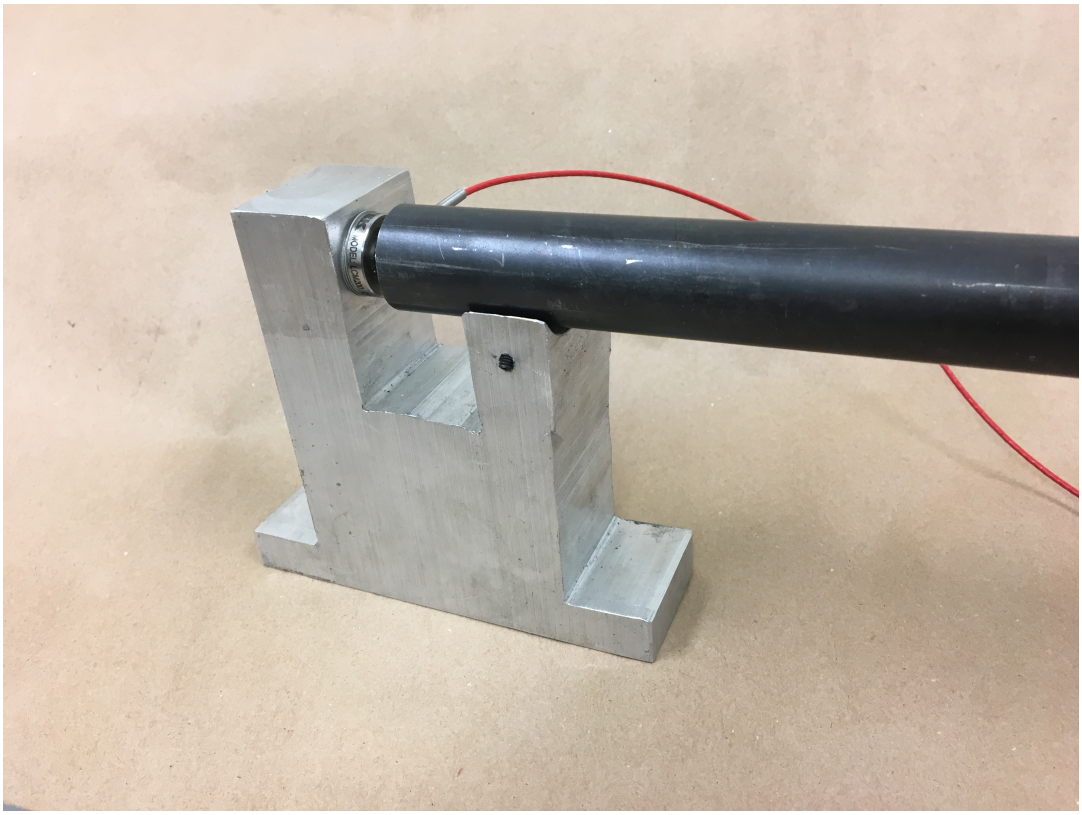

Figure 2.32: MKIII drag mounting block

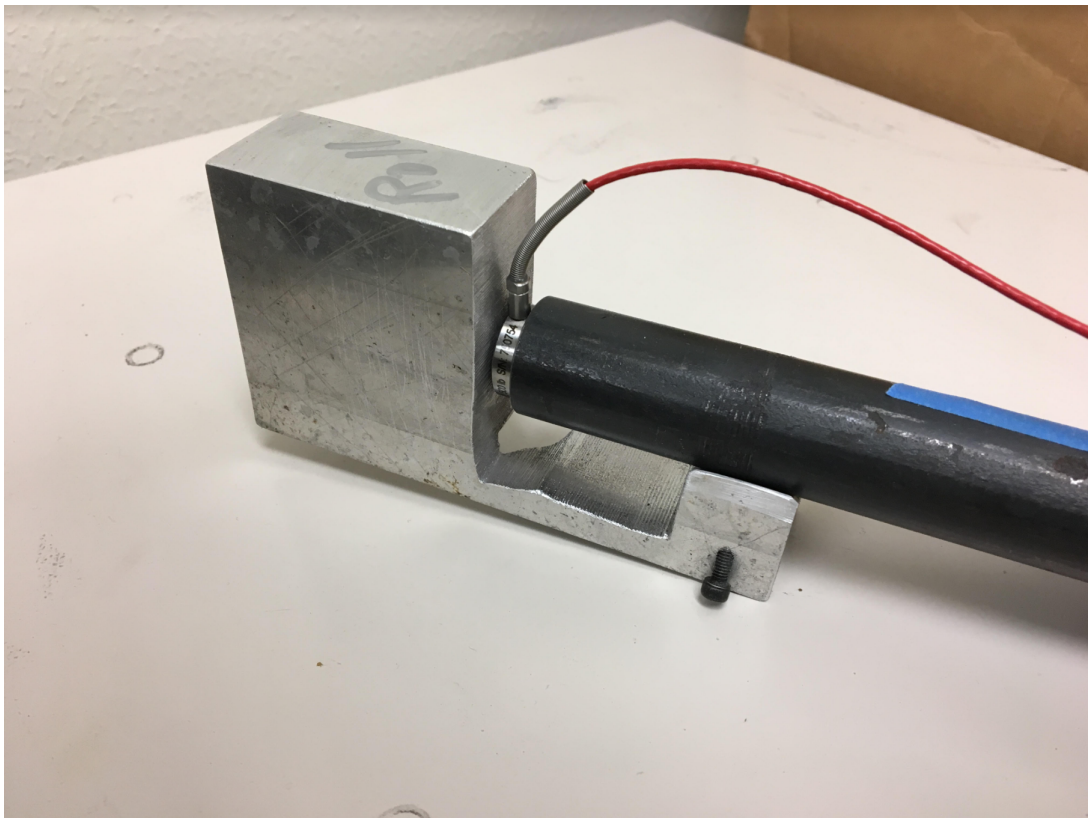

Figure 2.33: MKIII roll mounting block

In this configuration four of the six poise weight balances had been bypassed. Two of the three moments and two of the three forces were converted entirely to load cells, eliminating both the best and worst behaved poise weights of each set. Additionally, the remaining force and moment poise weights are substantially more difficult to access for installation and test using the usual system. For these reasons, this setup of four load cells was considered sufficient to judge the merit of the fully digital system, and so was investigated thoroughly. The results of these tests are presented below.

Loadup tests indicated that further eliminating poise weight balances decreased coupling, and that improved alignment decreased coupling. The follwing plots, as well as plots 4.4 through 4.2 depict the load up vs. the load down for a variety of conditions. In order to fully exercise the balance in all of its available directions, the load up-load down sequence used previously was repeated with the turntable rotated at the usual 0° offset from the wind direction, as well as 45° and 90° to measure a mix of pitch and roll, and pure roll, respectively. Additionally, a pulley system was used to both apply drag and thrust forces, as well as provide positive lift on the balance. An example of the data collected in these tests is presented in figure 4.4. However, comparing the load-up vs the load-down halves of each data-set and examining each direction independently presents not only the most complete picture of the loads on the balance in each test, but also highlights the any hysteresis in the system. These plots depict each component direction under a variety of loading conditions. This was done in order to flush out any hysteresis or coupling in the system. Each data series corresponds to one loading case, identified by the primary loading vector.

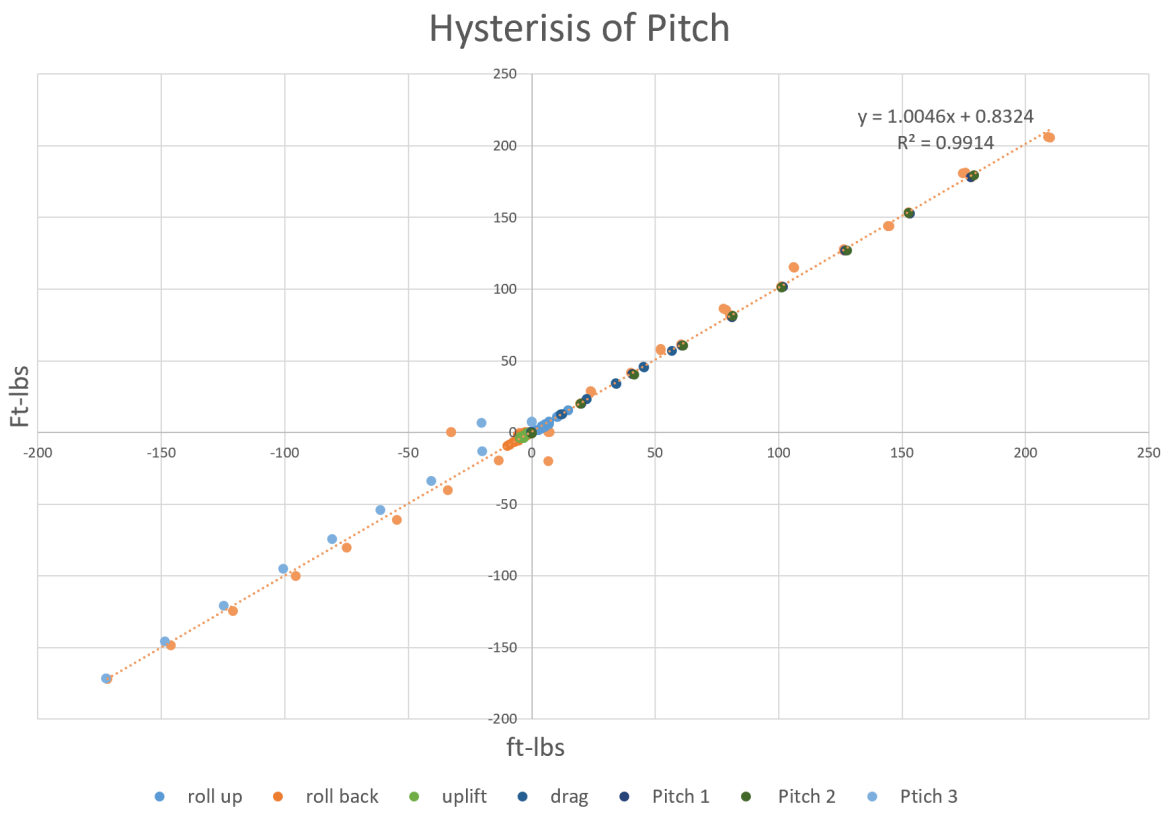

Figure 2.34: Final Pitch Loading and Hysteresis

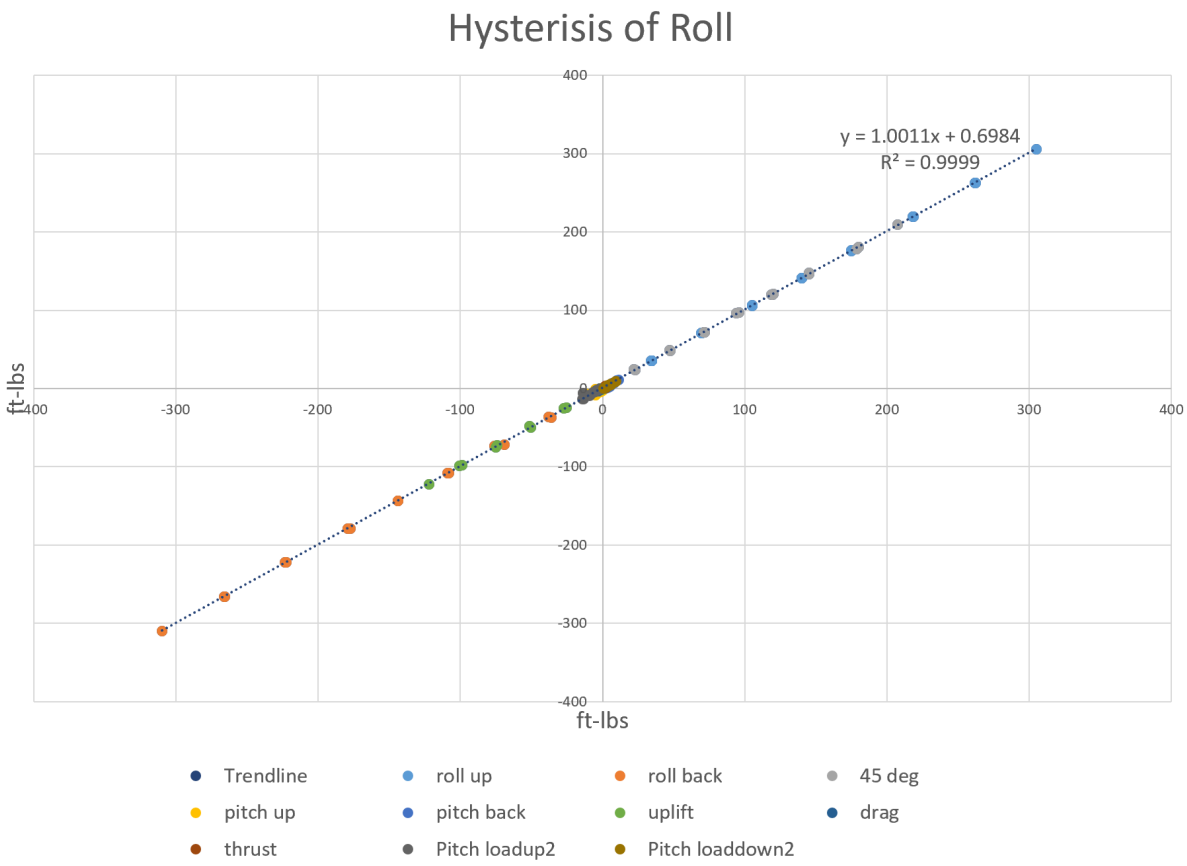

Figure 2.35: Final Roll Loading and Hysteresis

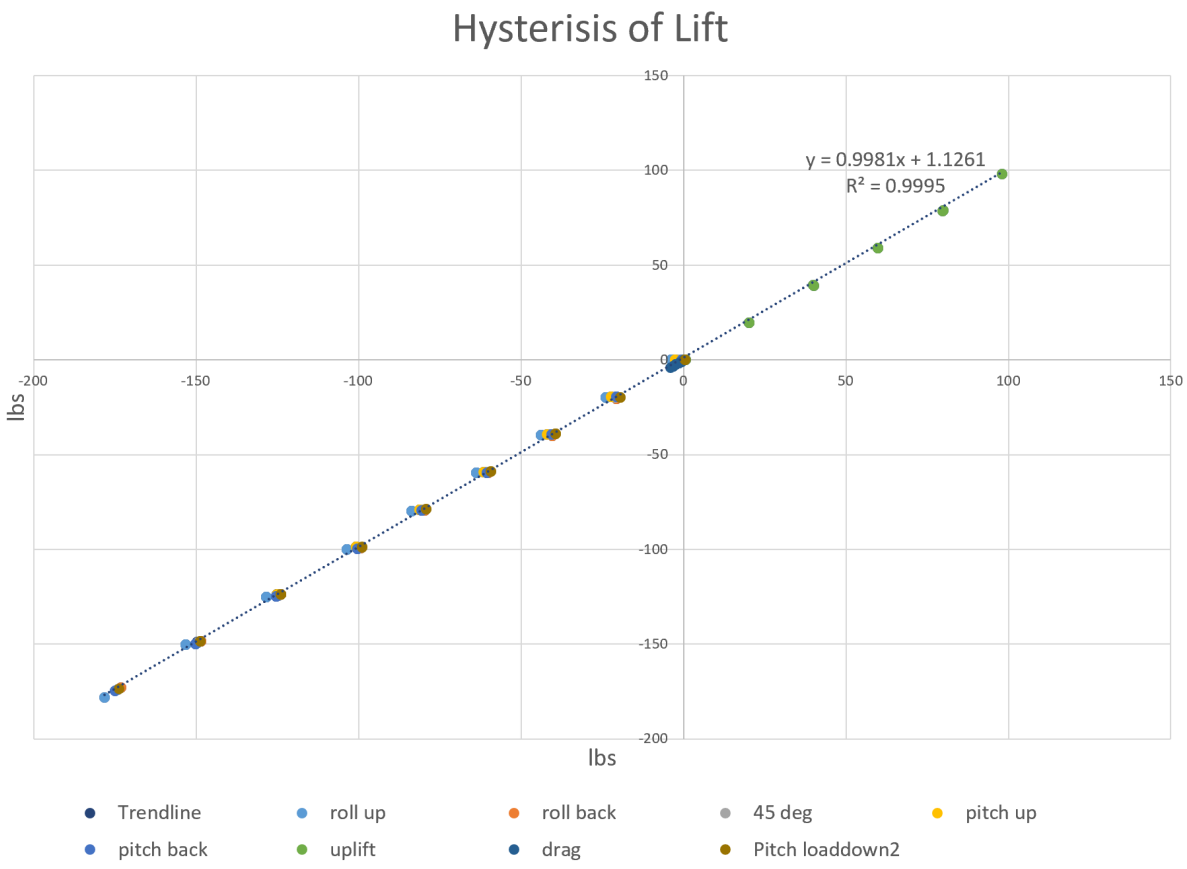

Figure 2.36: Final Lift Loading and Hysteresis

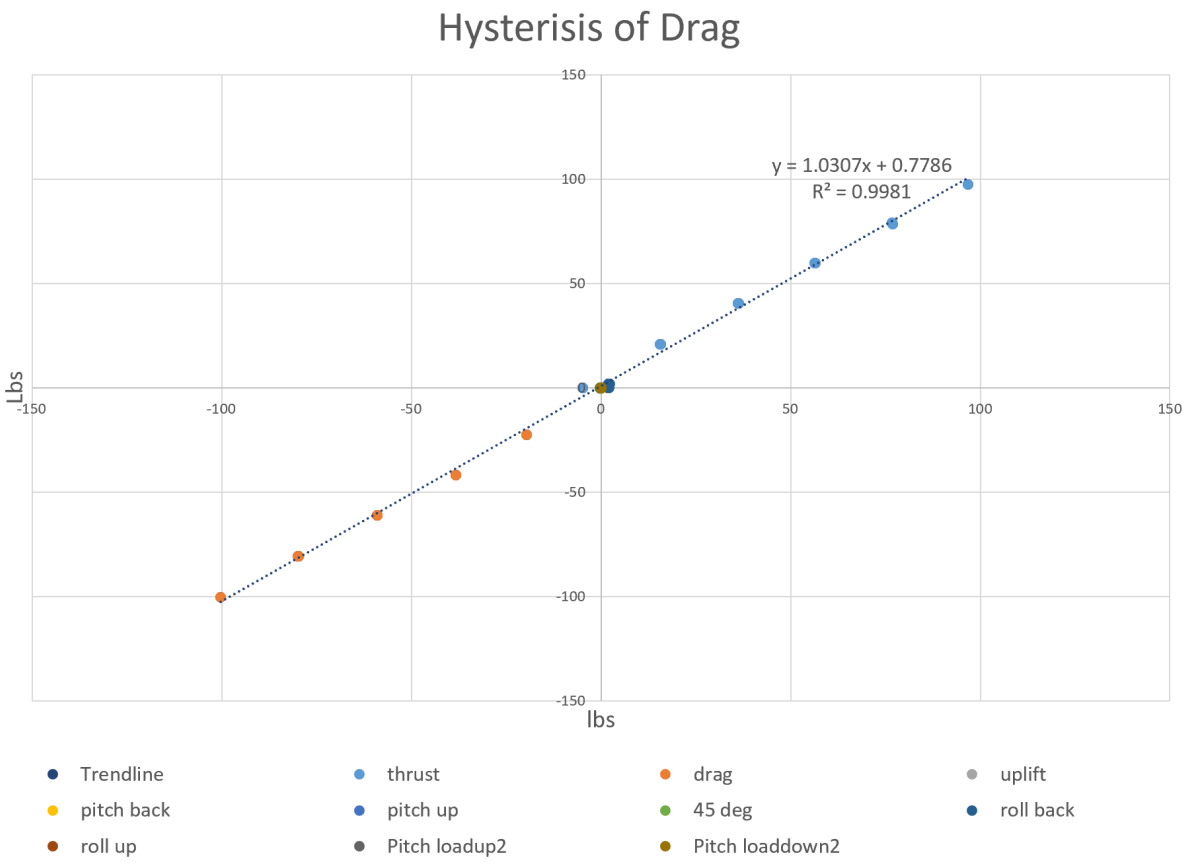

Figure 2.37: Final Drag Loading and Hysteresis

The results of a series of single point test are presented in figure 4.5. As before, these single point tests are intended to test the repeatability of the balance, and its ability to return to an known value. As indicated in the previous hysteresis plots, pitch struggles to return to the same value. However, roll, lift, and drag all return to their respective accepted values very well. This indicates that the hysteresis of pitch does affect the repeatability of pitch, but that the remaining three load cell systems are functioning quite repeatably.

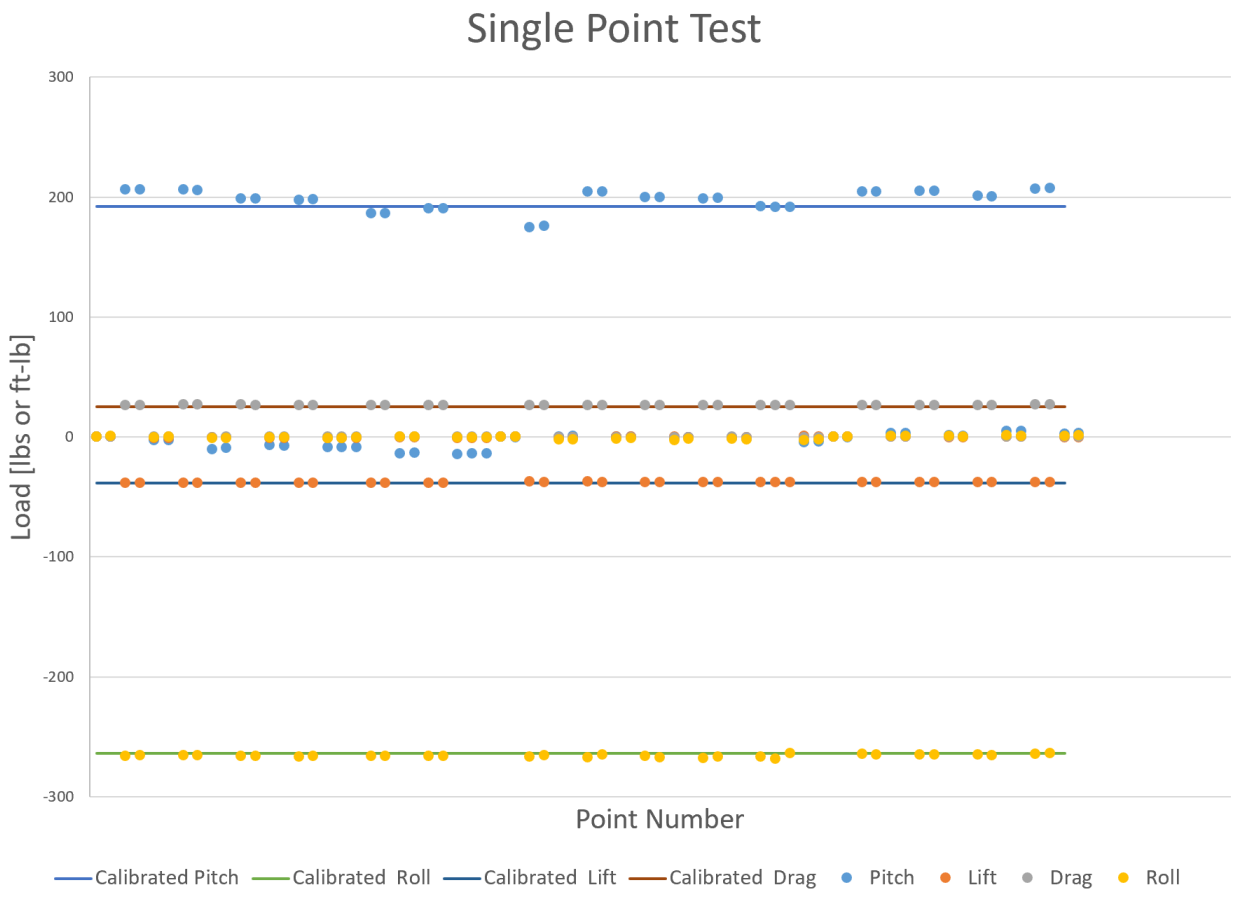

Figure 2.38: Final Single Point Test

An additional test was to simply allow the balance to collect data over time. This test was useful in determining the contributions of various factors on the noise of the system. Figure 2.39 illustrates some of the results of this tests.

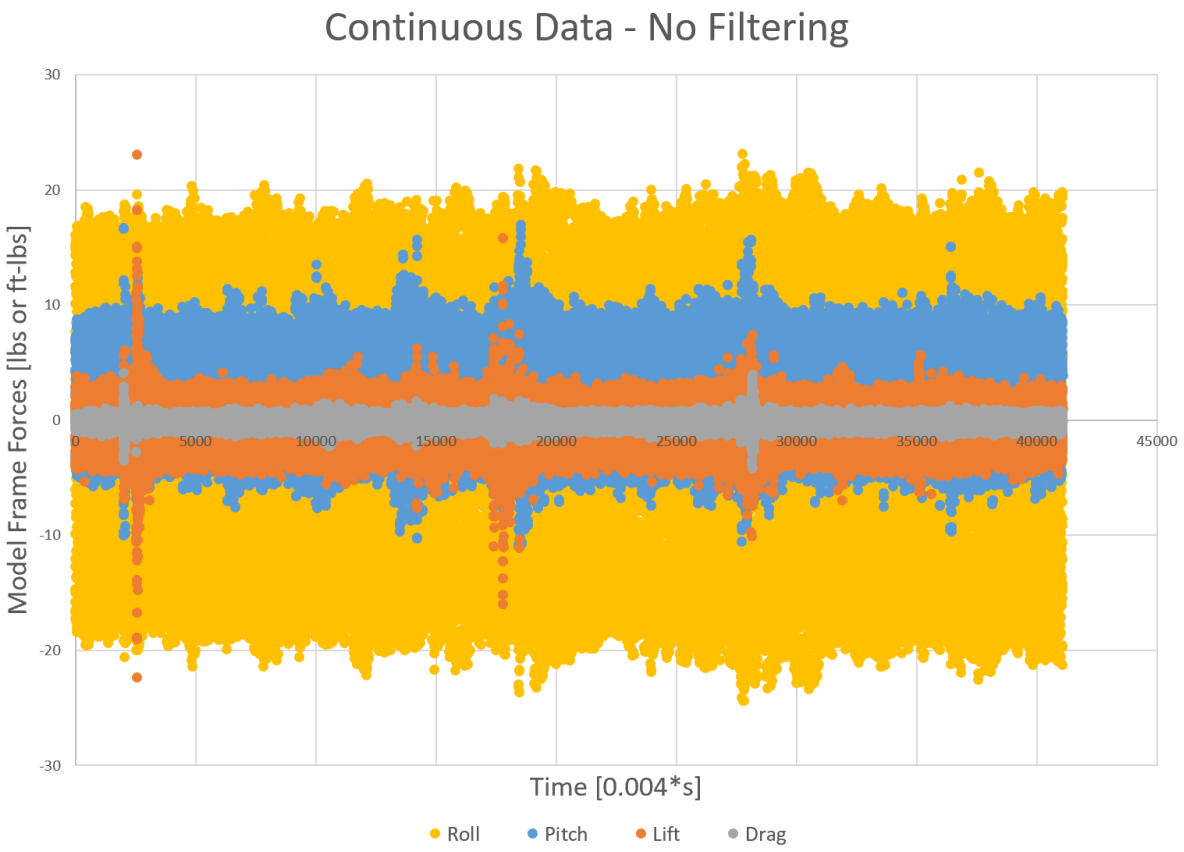

Figure 2.39: Baseline Noise in the MKIII System

It should be noted that there are a variety of spikes and other disturbances in this data. Some of these effects have been called out in the plots above, both to illustrate the precision of the balance, and also its sensitivity to disturbances. Because the balance is firmly affixed to the foundations of the building, any disturbances, especially sudden shocks, in or around the building are easily picked up by the balance. Slamming doors, runs in the adjoining hyper-sonic tunnels, or aircraft activities at the neighboring airport could all be seen in the stream of instantaneous data. This could indicate a potential problem, as the original poise weight balances were physical incapable of true instantaneous readings, the new system may be more susceptible to outside disturbances affecting the data. However, this risk can be easily mitigated by continuing to average one second of continuous data together to make a single data point. This method should effectively eliminate the effect of shock and high frequency disturbances. However, should instantaneous data be required from the balance, these factors should be taken under consideration.

Finally, a test was performed to see how well the digital balance system could hold a steady load over time. After loading the balance, the the standard one second of averaged continuous data was used for each of the data-points, and was allowed to collect data for approximately 30 minutes. After correcting for a gradual change in temperature as, the results were complied and are presented below in figure 4.6. This figure probably best illustrates the actual reliability and accuracy of the balance. The bands of data for each sensor show the margins for each axis of the balance.

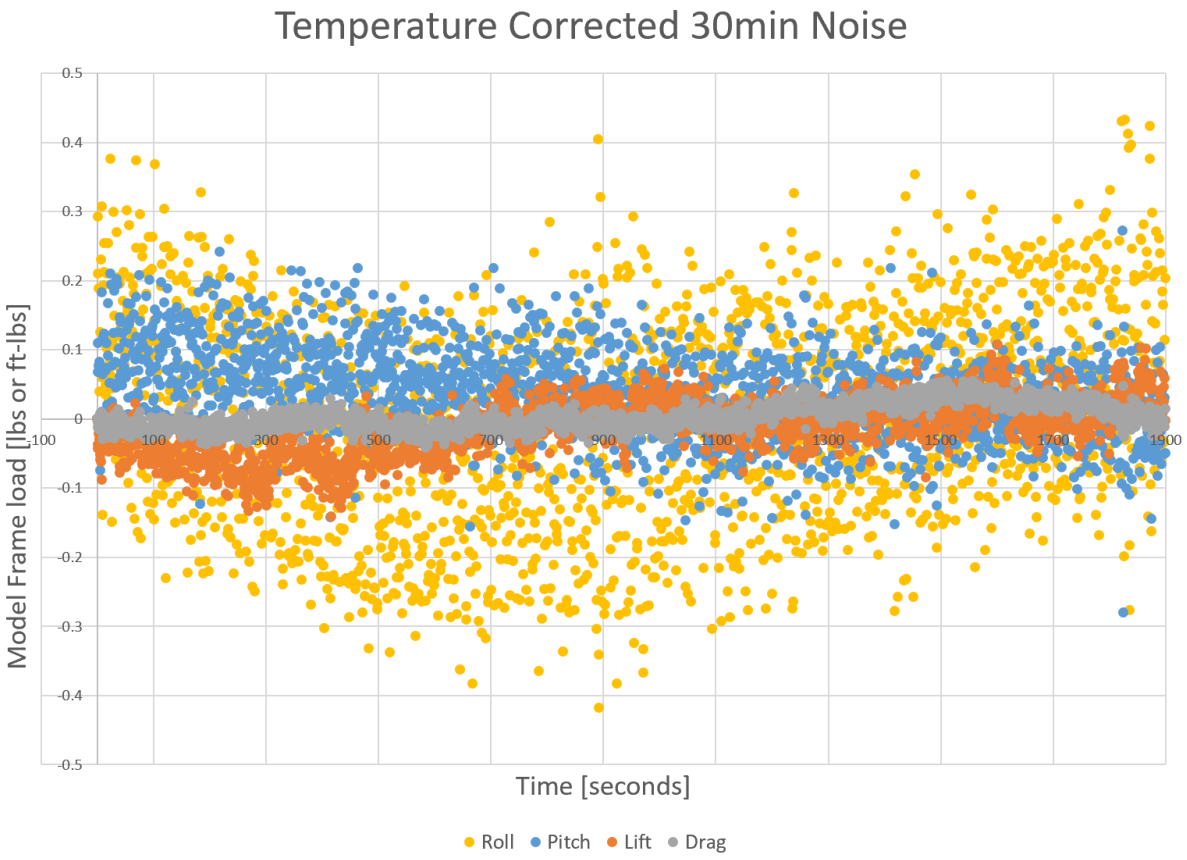

Figure 2.40: 30 min of Constant Load, MKIII design

3. CALIBRATION SCHEMES

3.1 Passive schemes

Because early versions of the the load cell mounting systems could be implemented without affecting the original analog balance beams, they could both be run simultaneously, and the data from the two sources could be compared. It was intended for data acquired during regularly scheduled commercial and academic tests to provide passive calibration data and characterize the performance of the load cells.

Unfortunate, this approach proved impossible. In order for both the poise weights and the load cells to be used, only the MKI or MKII designs could be used, but neither had sufficient accuracy or reliability to match poise weight data. Additionally, the noticeable bending in the pushrods observed in the MKI design raised concerns that the buckling could degrade performance of the existing system. Finally, in the few cases where it may have been feasible, the customer required the SCXi channels that were then being used for the balance load cells, meaning that load cell data could not be taken. For these reasons, while ideally they would have been used, passive calibrations were not used to test this system.

3.2 Active schemes

3.2.1 Single Point Data

The new balance system was instead calibrated using more explicit methods. The simplest, fastest, and most repeatable test was the single point test. In this test, a single weight is hung from a specific point on the balance that applies a load to each of the six sensors. This test is extremely well characterized, as it is used as the standard morning test to check the calibration for the analog balance beams for the past 70 years. The weight has remained unchanged since the 1970's and the hanging location is a fixed bracket with a removable pin. Because of the certainly with which the loading is known, the single point test serves as an excellent accuracy check. Additionally, because the balance can easily be loaded and unloaded with the removable pin system, it also serves as a

repeatability check. The Single Point system is illustrated in figure 3.1, with the weight suspended from the mounting point near the center of the balance. Figure 3.2 displays the single point test using the MKIII system, and is a duplication of the earlier figure.

Figure 3.1: Single Point Mounting System

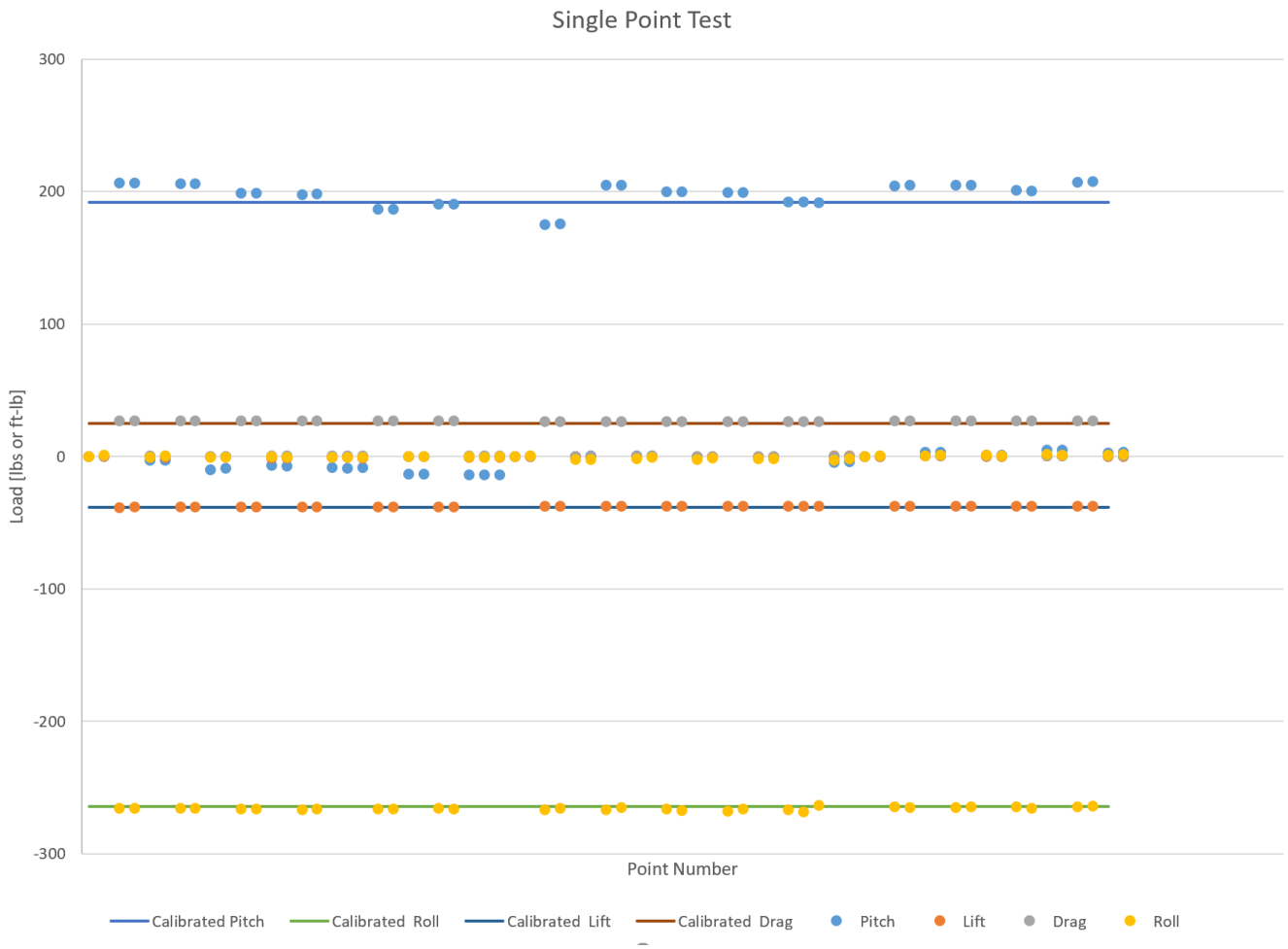

Figure 3.2: Comparison of single point data

3.2.2 Dumbbell Data

While the single point test is very convenient, it cannot establish the linearity of the system. For this, two different tests were used. The first was the dumbbell load up test, and the second was the full calibration developed by Stanford [**Stanford**]. For the dumbbell test, a set of five twenty-pound weights were stacked onto the external balance in the test section. This was an easy way to load the balance in incremental steps. However, only lift, roll, and pitch could be loaded in this configuration, shown in figure 3.3. Nevertheless, it served as an excellent method of testing the linearity of the balance, without extensive equipment installation.

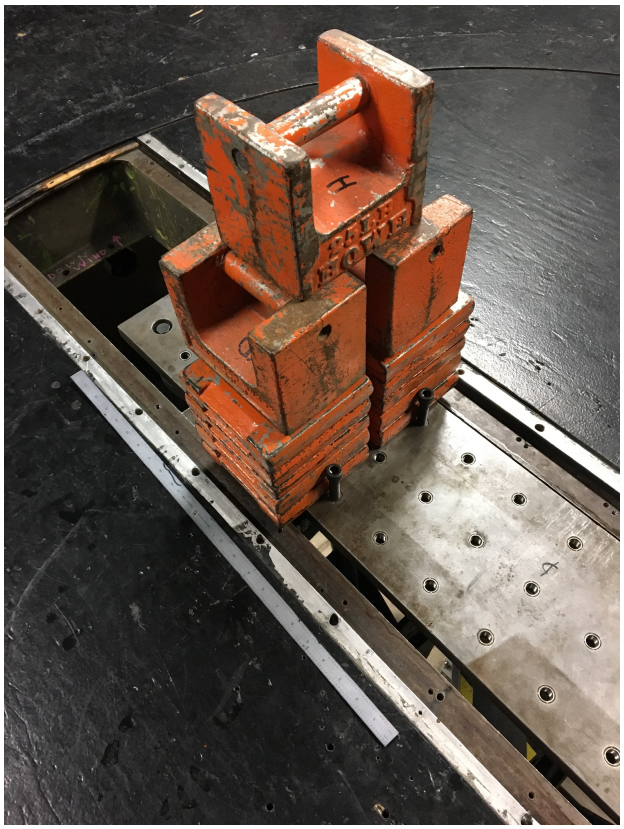

Figure 3.3: Dumbbell Loading in Pitch

With the addition of a pulley system, positive lift as well as positive and negative drag could also be tested. Figures 3.4 and 3.5 illustrate the arrangement of the pulley system. These two

arrangements allowed the balance to be tested in positive lift by pulling upwards on the balance, and positive and negative drag by pulling on a pole mounted in the center of the balance.

Figure 3.4: Dumbell Loading in Lift

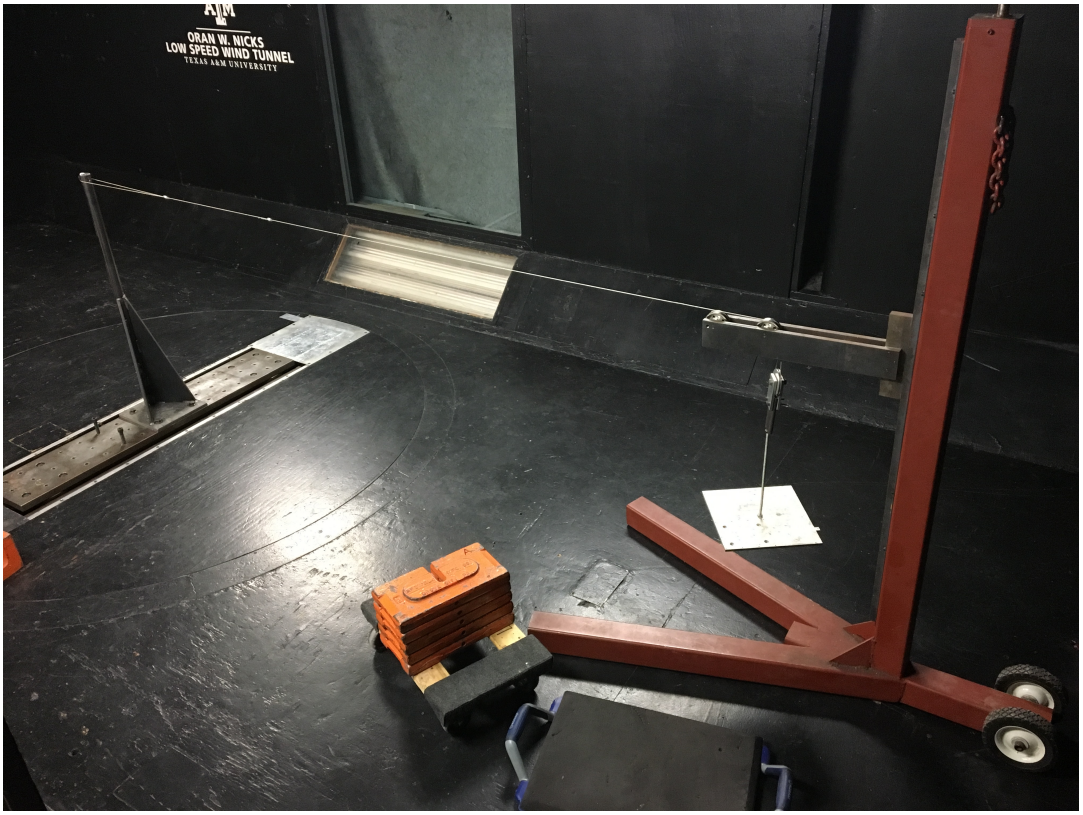

Figure 3.5: Dumbell Loading in Drag

3.2.3 Full Calibration

The last calibration method used is a full calibration. Developed by John Stanford for his master's thesis [**Stanford**], this calibration rig was designed to confirm the calibration of the original analog balance. However, because the new load cell system mounts models in the same way as original system, using the same pyramidal balance, it was easily re-purposed to test the load cells balance. The Stanford calibration approach, shown in figure 3.6, consists of a large cruciform rig affixed directly into the normal model mount. A hydraulic cylinder then applies a load to the rig through a load cell from various orientations on various positions on the rig. By comparing the load reported by the external balance to the load reported by the load cell on the hydraulic cylinder for each configuration, the full characteristics of the balance can be identified. This system has the advantage of being able to selectively load every axis of the external balance, but comes at the disadvantage of being difficult to install and use. Additionally, the nature of the hydraulic cylinder made it difficult to repeatably load the balance. Figure 3.7 shows the poise weight output of the Stanford calibration system for a test with two sequential load-up load-down cycles with the MKI load cell installed. The hysteresis results for this test are in figure 3.8, which is a duplication of a previous figure.

Due to the simplicity and ease of use, the dumbbell method of testing was used most often, with passive data being taken only sparingly, out of concern of damaging the load cells and corrupting the poise weight readings, and using the Stanford calibration rig only once, because the pulley system enabled lift and drag to be tested with the dumbbell system with considerably less effort.

Figure 3.6: Stanford Calibration mounting Rig

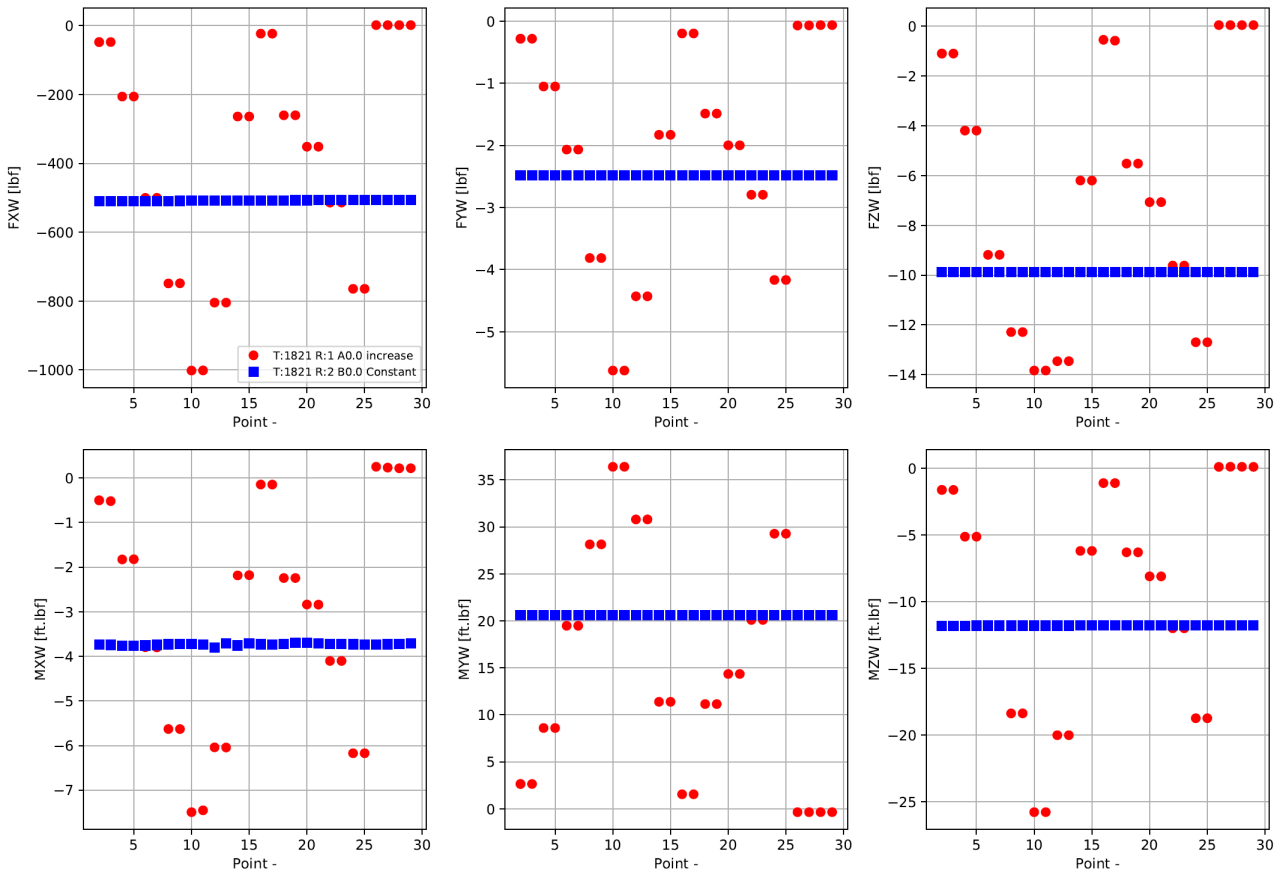

Figure 3.7: Stanford Calibration Data

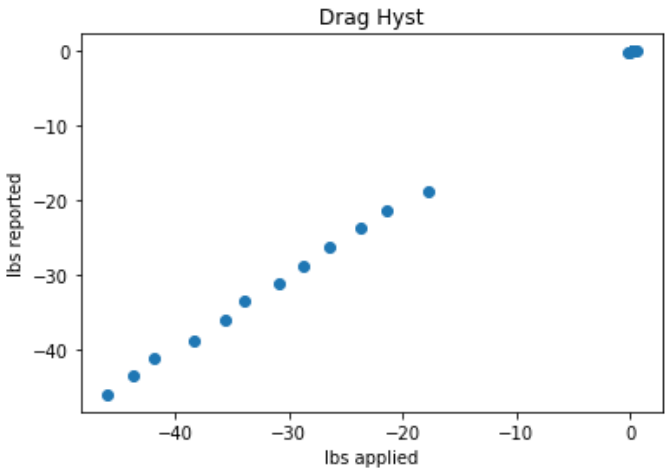

Figure 3.8: Drag hysteresis from Stanford Calibration

3.3 System Calibration

These techniques were used to evaluate the success of each iteration of the load cell systems. By comparing the applied load to the load reported by the load cell the linearity, hysteresis, repeat ability, and accuracy of each design could be determined and compared to each other and the original analog balance. The plots shown throughout section 2 present the results of these individual tests.

It should again be noted that the load cells have been implemented in the same location as the original analog balances, meaning that the mechanical advantage of the external balance must still be accounted for when translating the forces and moments of the load cells to the model frame. This was accomplished by multiplying the reported force from each load cell by a scaling factor unique to each force or moment system. These scaling factors were initially estimated by examining the lengths and positioning of each lever arm system. These estimates were confirmed with the single point test.

Overall, the final load cell system is largely decoupled with acceptable levels of hysteresis and accuracy. While, as mentioned in section 2, at the time of writing there is still some coupling and hysteresis, it is believed that these issues can be overcome with continued refinement of the current load cell scheme.

While each balance direction can be calibrated individually using the load up technique, there is only a partial guarantee that there is no coupling between directions. It is unlikely that there would be any major coupling, as the pyramidal balance mechanisms have remained unchanged from the decoupled analog balance system. However, once all six force and moment load cell systems have been implemented, a full calibration will be implemented to confirm and characterize the external balance calibration as a whole.

4. RESULTS, CONCLUSIONS, AND FUTURE WORK

4.1 Criteria Review

The goal of this project has been to substantially improve the testing capabilities of the Texas A&M Low Speed Wind Tunnel (LSWT) by developing a system capable of replacing the current poise weight system for the external balance with a modern system. The external balance is the primary sensor system of the LSWT, but has become more difficult to use and maintain. By replacing this system with modern sensors, the reliability and repairability of the external balance can be vastly improved. At the same time, other benefits can be achieved. These include decreased reaction time, improved hysteresis rejection, and improved sensor accuracy. After initially exploring using a digital PID control scheme to drive an updated poise weight system, it was determined that a load cell strain gauge system would achieve better results.

In order to judge if the load cell system had improved the LSWT, the following criteria were developed. First, in order to adequately replace the poise weight balance, the load cell system must at least match the current accuracy of the balance: 0.2 lbs in lift, drag, and side, and 0.2 ft-lbs in roll, pitch, and yaw. This constitutes the minimum standard by which the load cell system can be considered a success.

Beyond this requirement, the load cell system should be an improvement upon the analog poise weight system by being easier to repair and upgrade. It should be capable of reacting quickly to changes in model loading by reporting instantaneous loading, rather than shifting a poise weight until forces are balanced. Finally, it should be able to quicly revert to the poise weight system, should a problem be encountered and a backup system needed.

4.2 System Performance

The following figures demonstrate the linearity, hysteresis, repeatability, and variance of the MKIII version of the load cell system. Figures 4.1, 4.2, and 4.3 show the linearity and hysteresis of the lift, drag, and roll load cell setups, respectively. All of these show acceptable levels of hysteresis, as well as strong linearity. Figure 4.4 shows the linearity and hysteresis of the pitch load cell setup. While this shows more hysteresis than desired, it is believed that it can be reduced with more careful alignment of the system. Figure 4.5 depicts the results of a single point test, which checks the repeatability of the system. Lift, drag, and roll are within desired specifications. Pitch is not as repeatable as the other three, but that is likely a result of the hysteresis discussed above. These plots are identical to the MKIII results shown in section 2, but are posted again here for convenience.

Figure 4.6 shows the drift in sensor readings over time, after being corrected for temperature variations. In this plot the comparative stability of lift and drag are evident, as well as the greater noise of roll and pitch. It is interesting to note that, while pitch still has some hysteresis, it is roll that has the largest variance. This is interesting because, historically, the roll poise weight balance has always been the hardest to keep within specifications, requiring by far the most maintenance out of all the original balances. This suggests that the pyramidal balance itself may be sensitive to noise in some directions more than others.

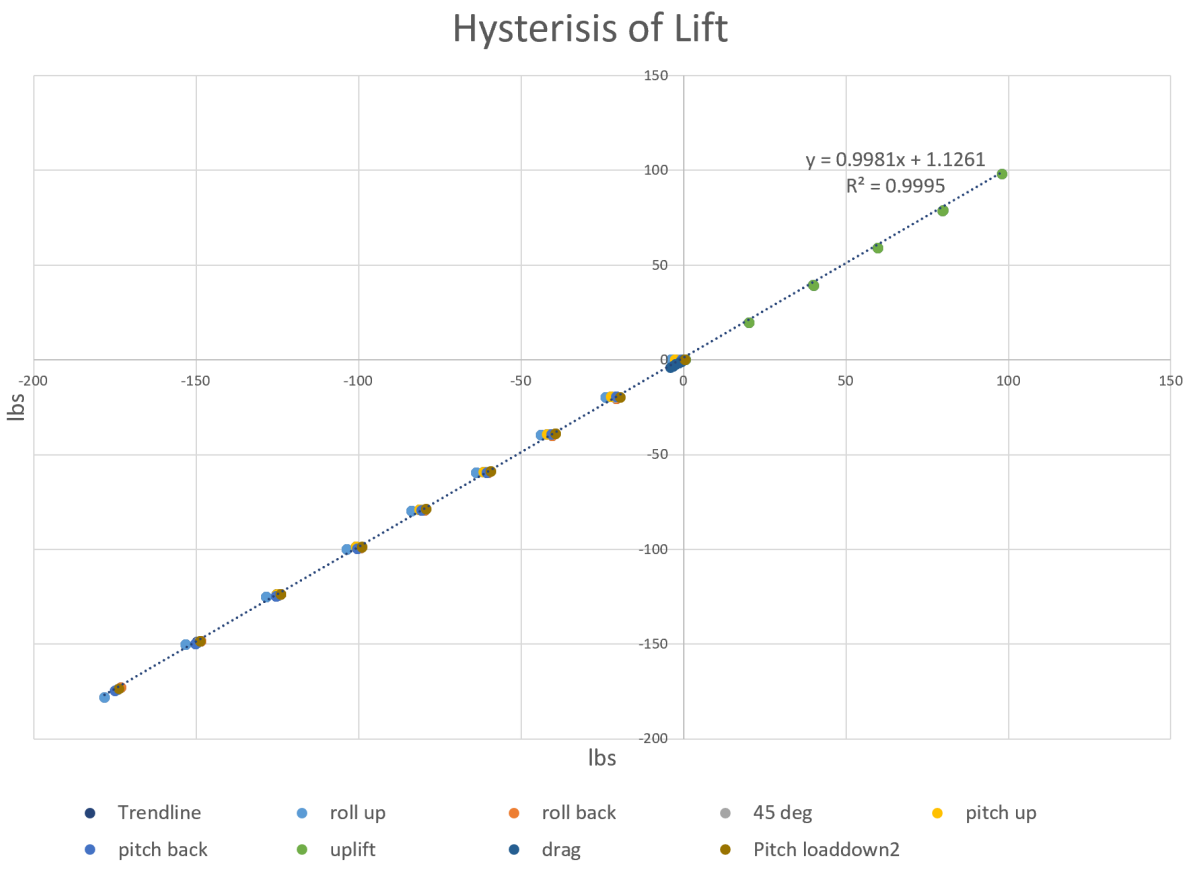

Figure 4.1: Final Lift Loading and Hysteresis

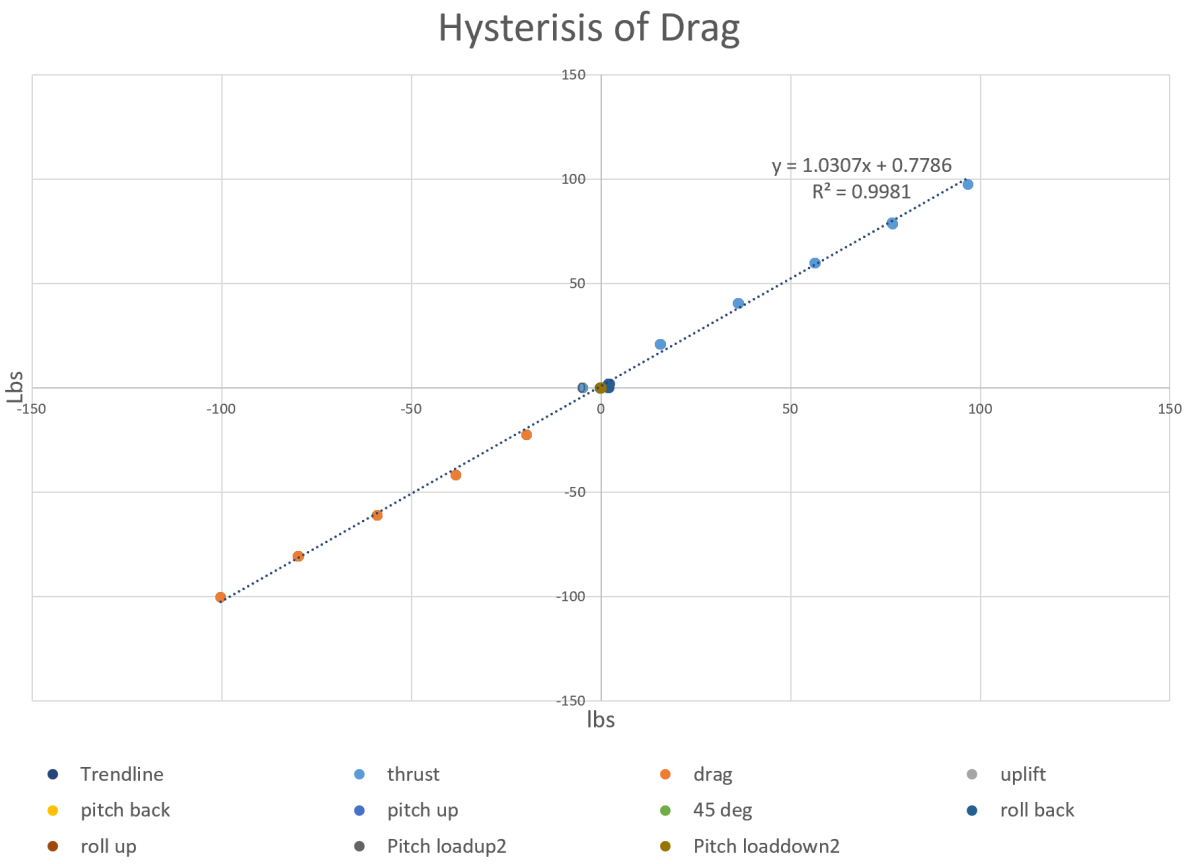

Figure 4.2: Final Drag Loading and Hysteresis

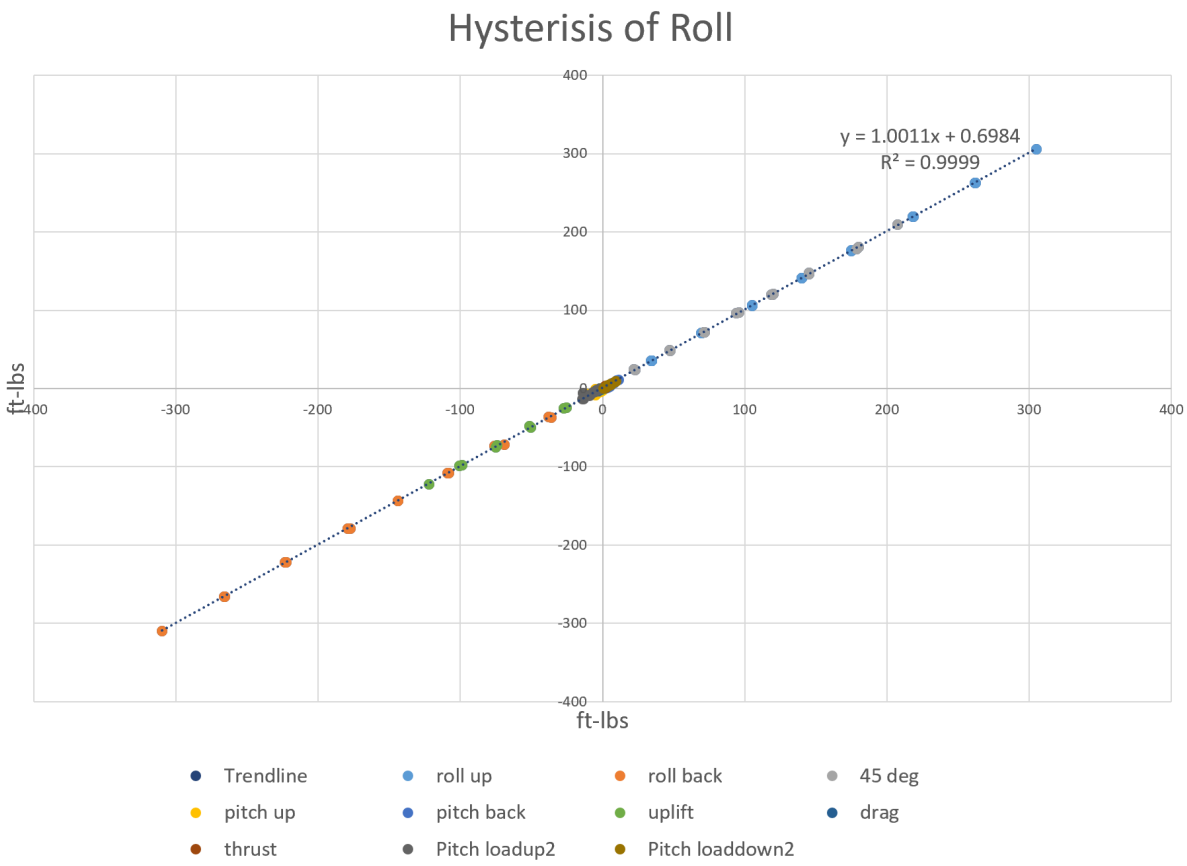

Figure 4.3: Final Roll Loading and Hysteresis

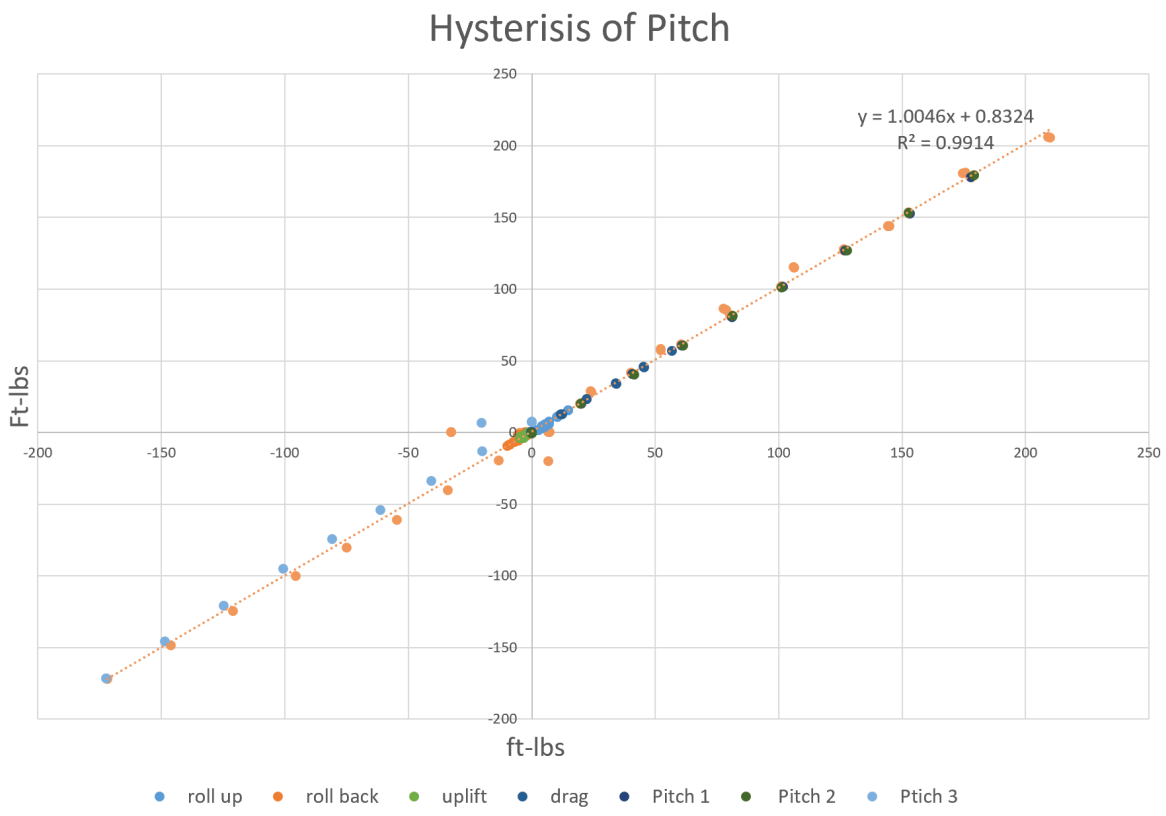

Figure 4.4: Final Pitch Loading and Hysteresis

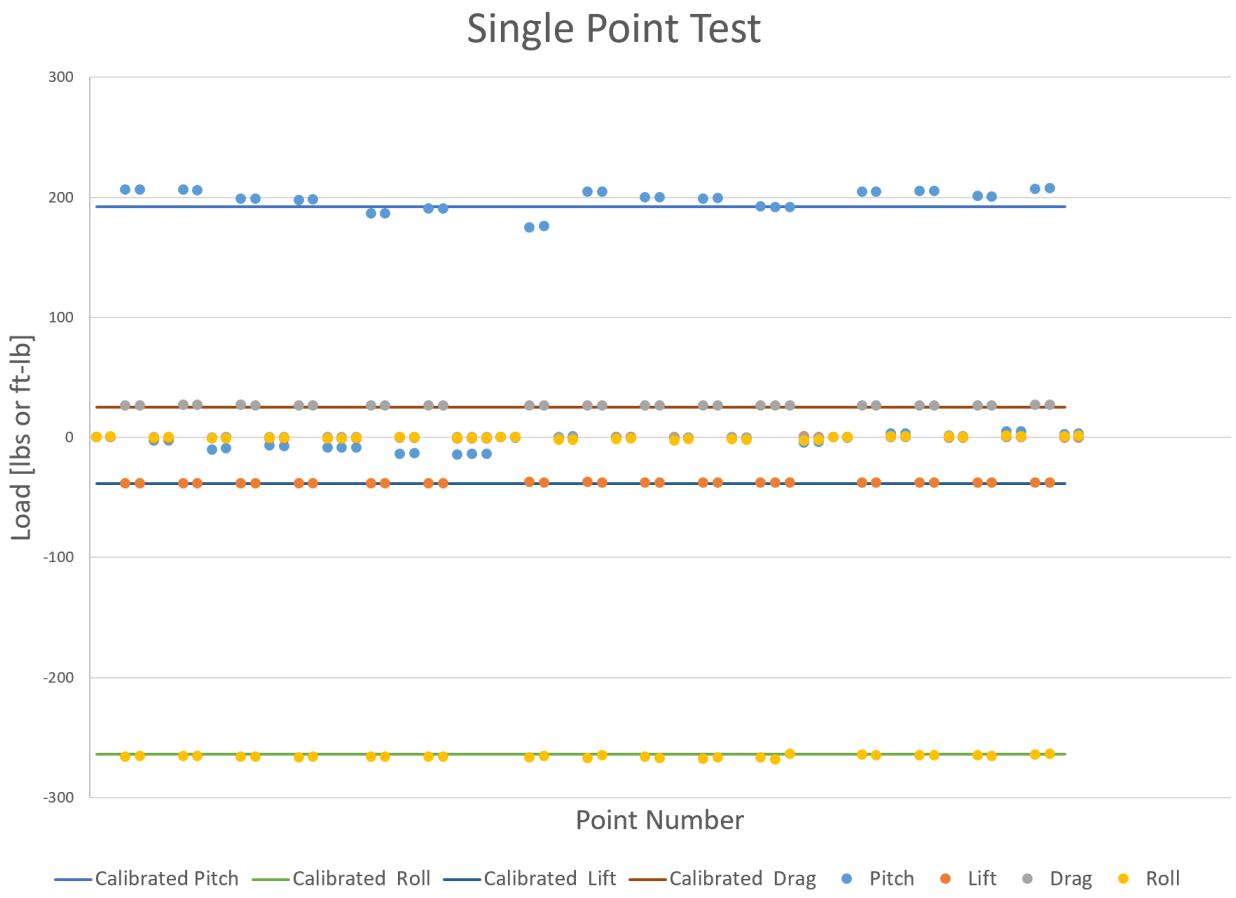

Figure 4.5: Final Single Point Test

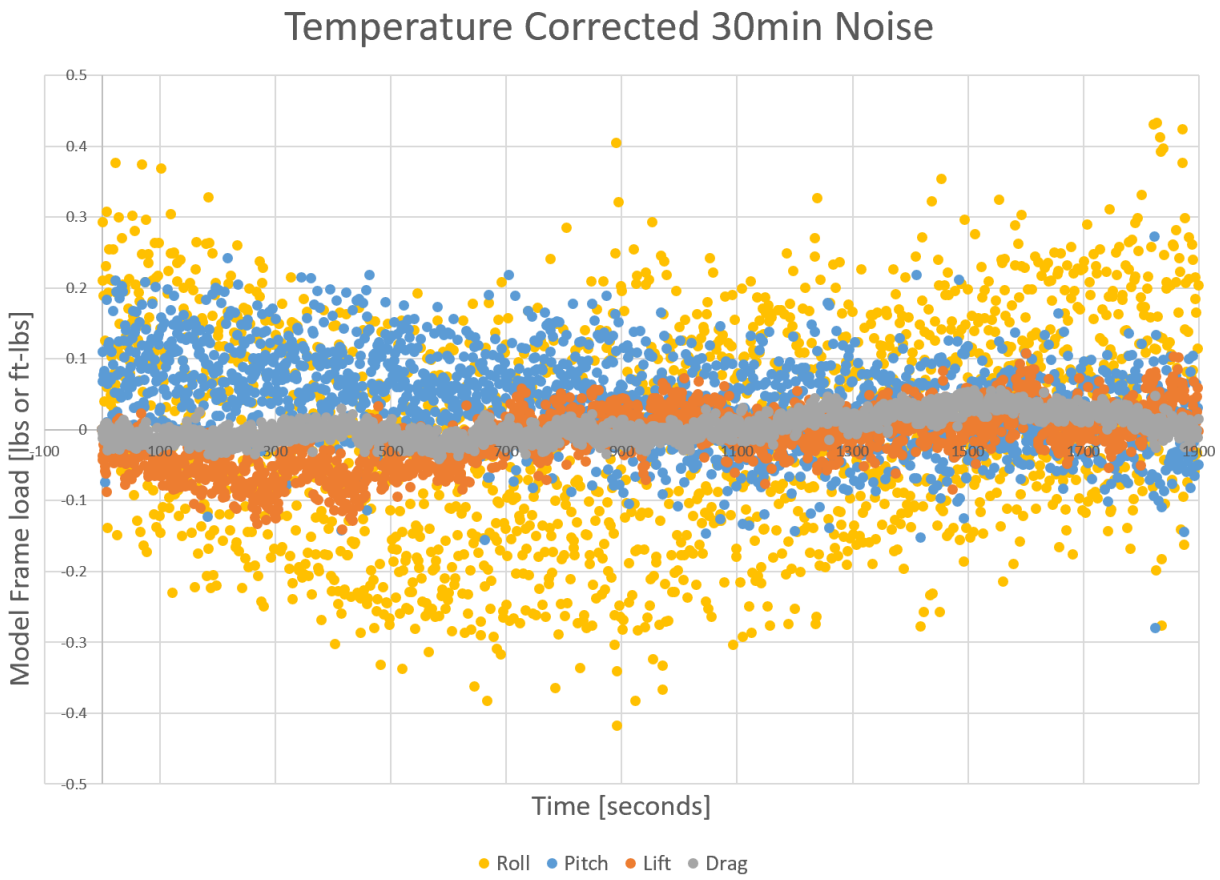

Figure 4.6: 30 min of Constant Load

4.3 System Results

In Summary, Table 4.1 lists the goals and requirements of this thesis, and the current status of each.

Table 4.1: Thesis Criteria Results

Quaility	Poiseweight Balance	Load Cell Balance
Model Frame Error	0.2 lbs	$\leq$ 0.2 lbs
Reaction Time*	17 seconds	Instantaneous
Hysteresis Rejection	Forced Overshoot	N/A
Data Rate	400 Hz	Variable, 1250 Hz standard
Replacement Ease	Very Difficult	Easy
Reversion Capable	N/A	Yes, 2 Hours

* Using Single Point tests as a benchmark

4.4 Future Work

First, and most critically, the remaining hysteresis in the pitch direction must be addressed. It is believed that this is due to slight misalignment of the pushrod, and may be relatively straightforward to resolve with better alignment.

The yaw and sideforce balances must be instrumented with load cells using designs similar to the MKIII designs currently used on the other four balance directions. This should also be a straightforward task. While these balances are less convenient to access, they are mechanically similar to the roll and drag balances, and so only slight modifications to those designs will be required.

After all directions are instrumented, each mounting block should be drilled and tapped down to the appropriate spots in order to make the arrangement both more permanent and more repeatable.

An additional feature that should be added is a notch filter to digitally eliminate frequencies known to have heavy noise, such as 60 Hz and its multiples.

While outside the scope of this thesis, other tasks related to this project include:

- Fully integrating this system into the LSWT DAQ computer network, which would allow for automatic data acquisition.
- Exploring the effects of temperature on the balance load cells, as well as other disturbances.
- Modifying the system to allow for smaller load cells to be swapped in. This would trade maximum loading range for improved accuracy in tests where accuracy is more needed than dynamic range.

BIBLIOGRAPHY

John W. Stanford III, “Calibration And Uncertainty Analysis Method for a Pyramidal External Balance”, Texas A&M University, 2016

Futek Advanced Sensor Technologies, LCM200 Specifications Sheet," Retrieved from http://www.futek.com/product.aspx?stock=FSH03904 Accessed: 2018-9-2.

National Instruments, PXIe-1071 Specifications Sheet," Retrieved from http://www.ni.com/en-us/support/model.pxie-1071.html Accessed: 2018-11-21.

Oriental Motor, Servomotors," Retrieved from https://www.orientalmotor.com/servo-motors/index.html Accessed: 2017-9-17.

Arduino, Arduino Uno information sheet," Retrieved from https://store.arduino.cc/usa/ arduino-uno-rev3 Accessed: 2017-9-17.

RDP Group, RDP electronics DCV Specifications Sheet," Retrieved from https://www.adminstrumentengineering.com.au/position-sensing-measurement/rdp-electronics-dcv Accessed: 2017-9-17.

APPENDIX A

ENGINEERING DRAWINGS

Contained in this section are engineering scetches and drawings for the vatious parts manufactured for this thesis

A.1 PID

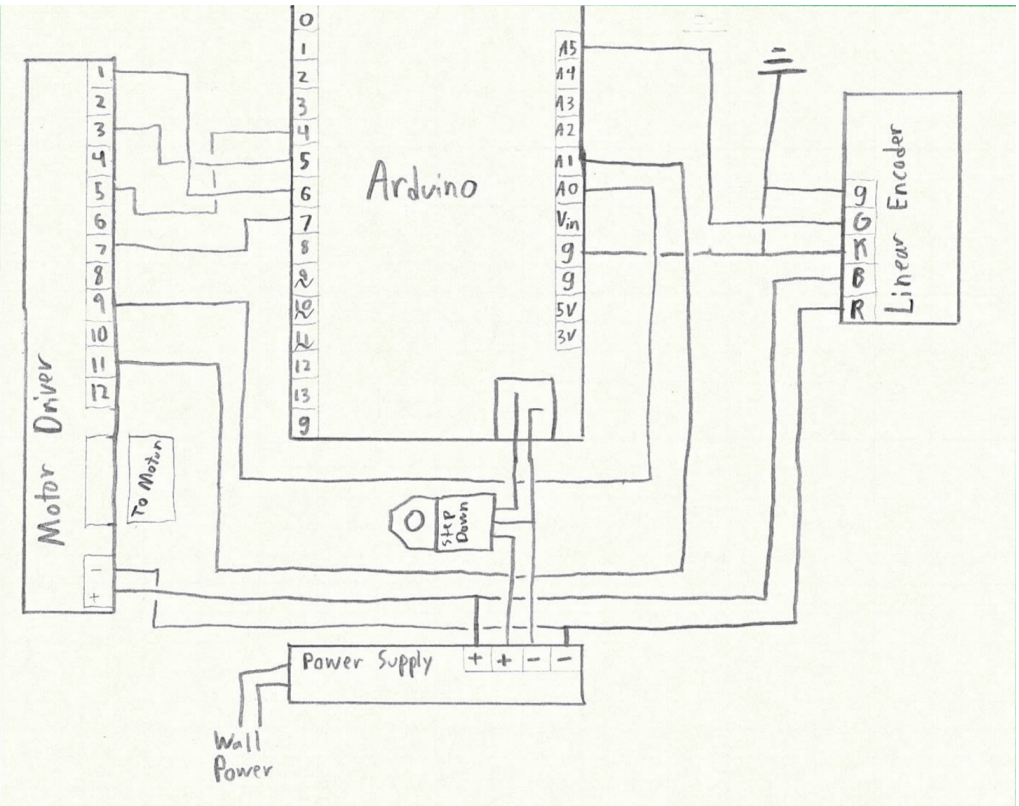

Figure A.1: Arduino wireing diagram

A.2 Pushrod MKI

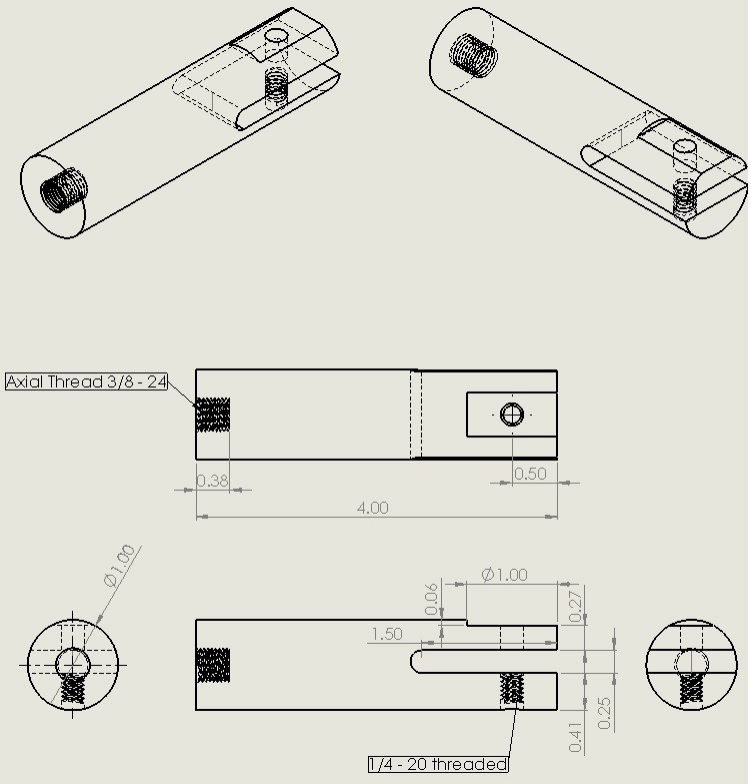

Figure A.2: MKI sketch

A.3 Pushrod MKII

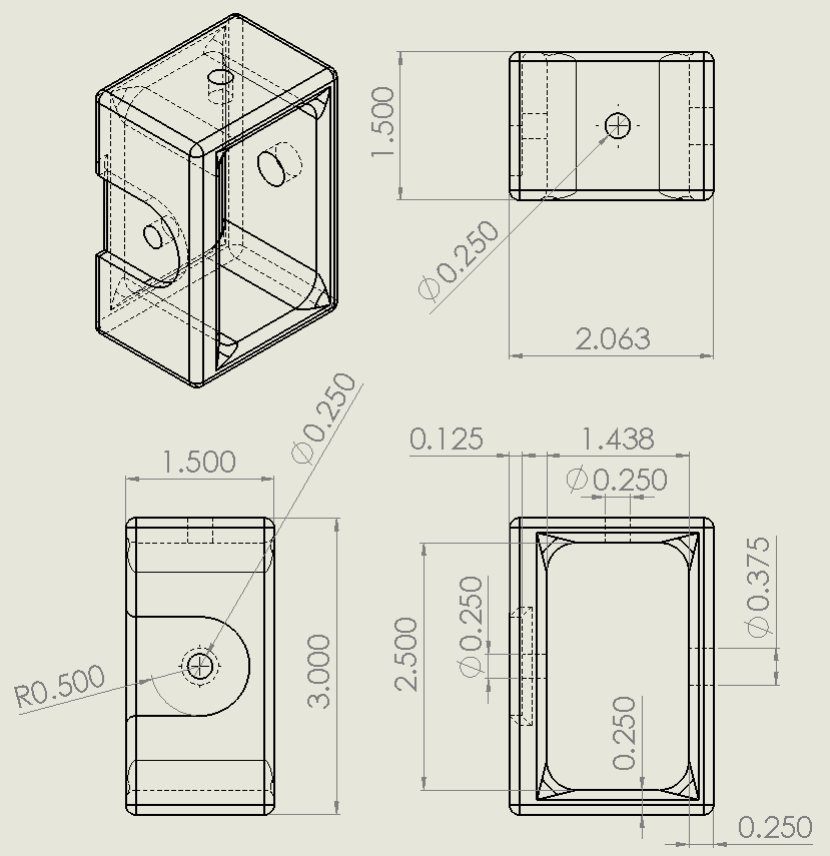

Figure A.3: MKII sketch

A.4 Pushrod MKIII

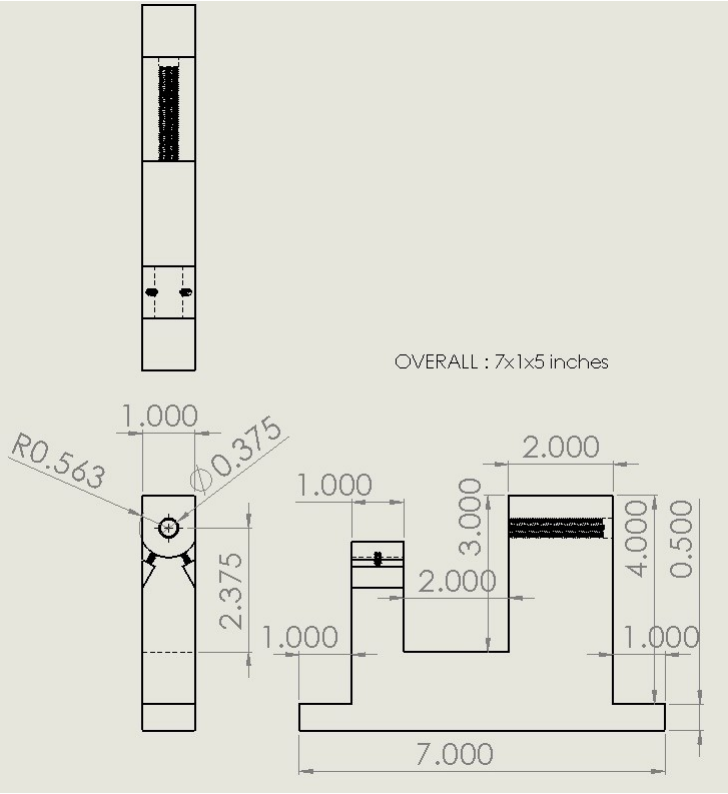

Figure A.4: MKIII drag sketch

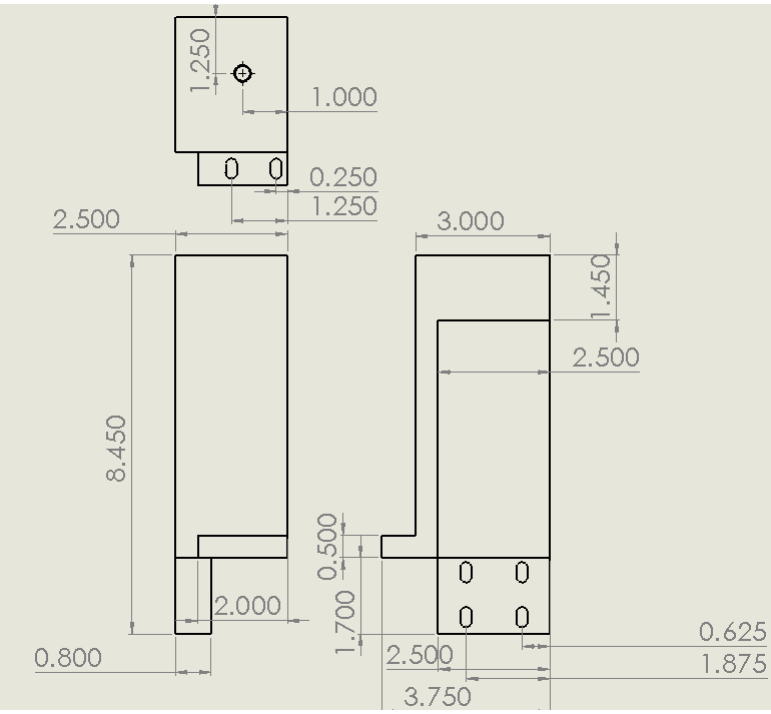

Figure A.5: MKIII lift sketch

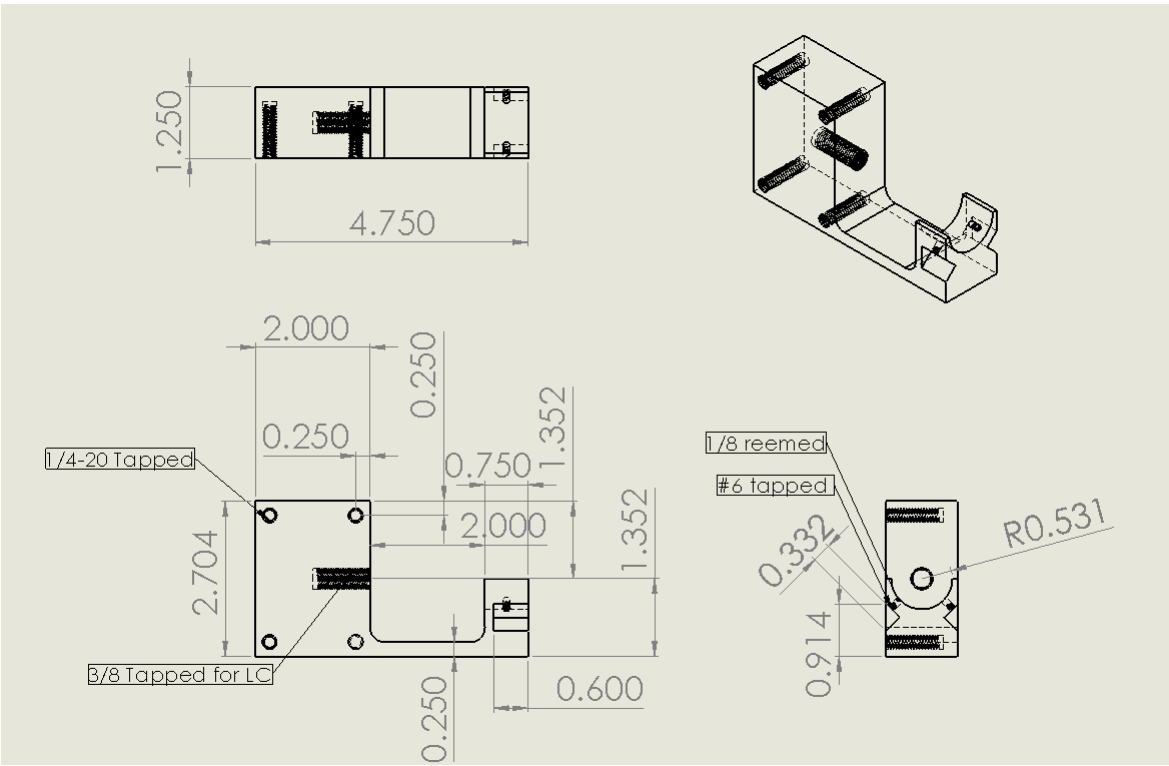

Figure A.6: MKIII pitch sketch